

# Multi-State Image Restoration by Transmission of Bit-Decomposed Data

Takashi Tadaki\*

*Department of Physics, Tokyo Institute of Technology,  
Oh-okayama, Meguro-ku, Tokyo 152-8551, Japan*

Jun-ichi Inoue†

*Complex Systems Engineering, Graduate School of Engineering,  
Hokkaido University, N13-W8, Kita-ku, Sapporo 8628, Japan*

(Dated: February 5, 2020)

We report on the restoration of gray-scale image when it is decomposed into a binary form before transmission. We assume that a gray-scale image expressed by a set of  $Q$ -Ising spins is first decomposed into an expression using Ising (binary) spins by means of the threshold division. We produce  $(Q - 1)$  binary Ising spins from a  $Q$ -Ising spin by the function  $F(\sigma_i - m) = 1$  if the input data  $\sigma_i \in \{0, \dots, Q - 1\}$  is  $\sigma_i \geq m$  and 0 otherwise, where  $m \in \{1, \dots, Q - 1\}$  is the threshold value. The effects of noise are different from the case where the raw  $Q$ -Ising values are sent. We investigate which is more effective to use the binary data for transmission or to send the raw  $Q$ -Ising values. By using the infinite range model, we first analyze the performance of our method quantitatively. Then we obtain the static and dynamical properties of restoration using the bit-decomposed data. In order to investigate what kind of original picture is efficiently restored by our method, the standard image in two dimensions is simulated by the mean-field annealing, and we compare the performance of our method with that using the  $Q$ -Ising form. We show that our method is more efficient than the one using the  $Q$ -Ising form when the original picture has large parts in which the nearest neighboring pixels take close values.

## I. INTRODUCTION

Statistical mechanical approaches to the problems in information science are employed frequently, and it is now known that such methods are very useful in various problems [1]. The method of statistical mechanics has been applied to many kinds of problems; for example, error-correcting codes [2, 3, 4], image restoration [5, 6, 7], problems related to economics [8, 9] and optimization problems [10, 11, 12]. Especially, the idea and method of the spin glass theory [13] have been applied to analyze the model of these problems. Recently, the performance of CDMA has also been estimated by the spin glass theory [14].

The image restoration problem has been investigated both theoretically and practically. We usually send and receive the information by means of various networks. The information is the data of document, sound, picture, and so on. However, it is generally impossible for a receiver to receive complete transmitted data when a sender transmits something, because the data are transmitted through a noisy channel. If we restrict the type of data to that of the picture, the original image is affected by some kind of noise when it is sent by a defective fax, a fickle e-mail, etc. When we receive such a corrupted image, we have to convert it using some kind of filter to obtain the original image. Basically it is the image restoration problem to estimate the original data (the original image) from the received, corrupted data (the degraded image). We may regard the digital picture as a discrete spin system. For example, a black and white image (WBI) corresponds to an Ising spin system by identifying the white color with +1 and the black with -1. Furthermore, the theory of image restoration is constructed by considering that two axes of the plane,  $x$ -axis and  $y$ -axis, correspond to two axes of time in the stochastic process. That is, the Markov process that the event occurs at a specific time is affected by what happened at neighboring pixels at a one-time step before.

---

\*Electronic address: tadaki@stat.phys.titech.ac.jp

†Electronic address: j'inoue@complex.eng.hokudai.ac.jp

The probability to determine what happens at a given time is derived from a priori knowledge which is obtained from a common sense of persons. The basic common sense is that the pixel's color is likely to be white if the color of neighboring pixels is white, and black otherwise. In other words, the pixel tends to take the same value as the neighboring pixels. However, the restoration of image by means of this knowledge only is not sufficient because the restored image becomes all white or all black just under the smoothing condition. Therefore we use the information of degraded image. Since the degraded image has not completely lost the information of the original image, we can reasonably construct the restoration process with the above a priori knowledge in addition to information of degraded image. This process can be written as a problem of statistical mechanics using Bayesian statistics, and the method of statistical mechanics can be applied to the image restoration.

There are mainly two standard approaches to the image restoration by means of the method of statistical mechanics. One is called the maximum a posteriori (MAP) estimation in which the estimation of the original image is given by maximizing a posterior probability distribution. This estimation will be seen to correspond to a search of the ground state of spin system described by the effective Hamiltonian in the context of statistical mechanics. Another is the estimation in which we regard the expectation value with respect to the maximized marginal posterior probability at each site in thermal equilibrium as the original image and is called the maximum posteriori marginal (MPM) estimation. This estimation is also called the finite temperature restoration. Therefore, the MPM estimation includes the MAP estimation. Among the two estimations, it was proposed by Marroquin et al [15] that the MPM estimation gives better performance than the MAP estimation. Nishimori and Wong [16] proved this fact for black and white images using a rigorous inequality. With respect to the gray-scale image, the same has been shown by Tanaka [17] from a different viewpoint.

Not only black and white images but also gray scale images are actively investigated by many people in the field of statistical mechanics. The pixel in the gray scale image takes discrete  $Q$ -state values and may be described in terms of Potts [18, 19] or  $Q$ -Ising spins [20]. Restoration of gray scale image using chiral Potts spin [21] may not be appropriate since chiral Potts spin can not express the distance among different states. However  $Q$ -Ising spin can express the gray scale level at least. Restoration of gray scale image using  $Q$ -Ising spin was first investigated by Inoue and Carlucci [22]. In their paper, restoration of gray-scale image expressed by  $Q$ -Ising spins was analyzed in the infinite-range model. Performance and properties of restoration were obtained quantitatively. Realistic images were also restored by means of Monte Carlo method and mean-field annealing. They also improved the restoration of gray-scale image by introducing a spin glass term which is called the parity-check term in the field of error-correcting codes.

We investigate the restoration of the gray scale image expressed by the  $Q$ -Ising spin when it is decomposed into the Ising spin before transmission. In this method, the gray scale image is decomposed into binary data by means of the method of threshold division before it is transmitted. Then the bit-decomposed data is transmitted through a noisy channel. Therefore the effects of noise is different from those in the  $Q$ -Ising form. We show how well the original image is restored in our method in comparison to the restoration using the  $Q$ -Ising form.

This paper is organized as follows. In the next section, we explain the general formulation of image restoration and the method of threshold division. In Sec. III, we analyze the static and dynamical properties of image restoration in the infinite-range model. In Sec. IV, we verify the result of the infinite-range model in realistic pictures by means of Monte Carlo simulation. In Sec. V, standard image is restored by the method of mean-field annealing. The performance of restoration in our method is compared with that using the  $Q$ -Ising form. The final section is denoted to summary and discussions.

## II. GENERAL FORMULATION

### A. Image restoration

A gray scale image is represented by a set  $\{\xi\}_{i=1,\dots,N}$  of fixed values. The variable  $\xi_i$  takes an integer value between 0 and  $Q - 1$ . Even in black and white image in addition to gray scale image, most of natural images have nontrivial structures generally. Therefore, it is impossible to discuss the property of a given specific natural image exactly. Nevertheless we may notice that an eminent property of natural

images is local smoothness. Therefore we assume that the original image is generated by the Boltzmann probability represented by the following:

$$P_s(\{\xi\}) = \frac{1}{Z(\beta_s)} \exp \left[ -\frac{\beta_s}{2z} \sum_{(ij)} (\xi_i - \xi_j)^2 \right], \quad (1)$$

where  $(ij)$  represents interacting sites and  $z$  is the coordination number.  $Z(\beta_s)$  is the normalization constant, and  $\beta_s (= T_s^{-1})$  is the inverse temperature to generate the original image. If  $\beta_s$  is large, an original image with many clusters consisting of the same value is generated.

A degraded image is generated by sending data of the original image through a noisy channel. We consider two kinds of noise in this thesis. One is the binary noise caused by a binary symmetric channel (BSC) and another is the Gaussian noise caused by the Gaussian channel (GC).

### 1 Gaussian channel

In the Gaussian channel, the output  $\tau_i$  for an input  $\xi_i$  is a Gaussian random variable with mean  $\tau_0 \xi_i$  and variance  $\tau^2$ . The probability distribution of output given the input  $\{\xi\}$  is written as

$$P(\{\tau\}|\{\xi\}) = \frac{1}{\sqrt{2\pi}\tau} \exp \left[ -\frac{1}{2\tau^2} \sum_i (\tau_i - \tau_0 \xi_i)^2 \right]. \quad (2)$$

The degraded image  $\{\tau\}_{i=1,\dots,N}$  is generated by this probability distribution.

Here, we consider about the Bayes formula. It gives the posterior probability distribution which is necessary to restore the original image. When there are two independent events,  $e1$  and  $e2$ , each other, the probability that these events occur simultaneously is generally represented as  $P(e1, e2)$ . The conditional probability that the event  $e1$  (or  $e2$ ) occurs after the event  $e2$  (or  $e1$ ) occurred is given by the probability  $P(e1|e2)$  (or  $P(e2|e1)$ ). The relation between these probabilities becomes

$$P(e1, e2) = P(e1|e2)P(e2) = P(e2|e1)P(e1).$$

Therefore we obtain the following expression.

$$P(e1|e2) = \frac{P(e2|e1)P(e1)}{P(e2)} = \frac{P(e2|e1)P(e1)}{\sum_{e1} P(e2|e1)P(e1)}.$$

This expression is called the Bayes formula. According to the Bayes formula, the posterior probability  $P(\{\sigma\}|\{\tau\})$  that the estimate of source sequence, namely the restored image, is  $\{\sigma\}_{i=1,\dots,N}$ , provided that the output is  $\{\tau\}$ , is given as

$$\begin{aligned} P(\{\sigma\}|\{\tau\}) &= \frac{P(\{\tau\}|\{\sigma\})P_m(\{\sigma\})}{\text{tr}_{\{\sigma\}} P(\{\tau\}|\{\sigma\})P_m(\{\sigma\})} \\ &\sim \exp \left( -h \sum_i (\sigma_i - \tau_i)^2 - \frac{\beta_m}{2z} \sum_{ij} (\sigma_i - \sigma_j)^2 \right) \\ &\equiv \exp(-\mathcal{H}_G). \end{aligned} \quad (3)$$

Since we can get the degraded image only and do not know the other information of original image, we introduced the model prior  $P_m(\{\sigma\})$  to represent a priori knowledge on natural image:  $P_s(\{\xi\})$  represented by equation (1). Furthermore prior parameters  $\beta_s$  and  $\tau_0/\tau^2$  to control the generation of original image and degraded image, respectively, are unknown quantities. Accordingly, we have to use the so-called hyper-parameters  $\beta_m$  and  $h$  instead of prior parameters  $\beta_s$  and  $\tau_0/\tau^2$ . Then, controlling these hyper-parameters, we can obtain the optimal restored image.

## 2 Binary symmetric channel

When binary data  $\{\xi_b\}$  ( $Q = 2$ ) takes 0 or 1, the type of noise can also be binary. In such a case, a pixel of the original image is flipped with the probability  $p$ , the error rate. The error probabilities of flipping the signal +1 to 0 and 0 to +1 are the same. The probability distribution of this output  $\{\tau_b\} \in \{0, 1\}$  is expressed as follows.

$$P(\{\tau_b\}|\{\xi_b\}) = \frac{1}{Z_\tau} \exp \left[ -\beta_\tau \sum_i (\tau_{i,b} - \xi_{i,b})^2 \right], \quad (4)$$

where

$$\begin{aligned} Z_\tau &= \text{Tr}_{\tau_b} \exp \left[ -\beta_\tau \sum_i (\tau_{i,b} - \xi_{i,b})^2 \right] \\ &= [1 + e^{\beta_\tau}]^N. \end{aligned}$$

The parameter  $\beta_\tau$  is defined by  $p$  becomes

$$\beta_\tau = \ln \frac{1-p}{p}. \quad (5)$$

The posterior probability in this case is

$$\begin{aligned} P(\{\sigma_b\}|\{\tau_b\}) &= \frac{P(\{\tau_b\}|\{\sigma_b\})P_m(\{\sigma_b\})}{\text{tr}_{\sigma_b} P(\{\tau_b\}|\{\sigma_b\})P_m(\{\sigma_b\})} \\ &\sim \exp \left( -h \sum_i (\sigma_{i,b} - \tau_{i,b})^2 - \frac{\beta_m}{2z} \sum_{ij} (\sigma_{i,b} - \sigma_{j,b})^2 \right) \\ &\equiv \exp(-\mathcal{H}_B). \end{aligned} \quad (6)$$

### B. MPM estimation and mean square error

Next, we discuss the method to estimate the original image from the preceding posterior probability distribution and to evaluate the restored image which is obtained by such estimations.

We consider the marginal distribution obtained from the posterior probability distribution equation (3) (or (6)) to estimate the original image:

$$\bar{P}(\sigma_i|\{\tau\}) \equiv \sum_{\sigma \neq \sigma_i} P(\{\sigma\}|\{\tau\}) \quad (7)$$

Using this marginal probability distribution, we can calculate the local magnetization at a site  $i$  as given by

$$\langle \sigma_i \rangle_{\beta_m, h} \equiv \sum_{\sigma_i=0}^{Q-1} \sigma_i \bar{P}(\sigma_i|\{\tau\}). \quad (8)$$

Since the above expectation value is a continuous real number, we need to change it into an integer by means of the following function  $\Omega$ : because the original image consists of the discrete value in digital images, the restored image is the estimation of original image should, properly, take the discrete value.

$$\Omega(\langle \sigma_i \rangle_{\beta_m, h}) \equiv \sum_{k=1}^Q k \left[ \Theta \left( \langle \sigma_i \rangle_{\beta_m, h} - \frac{2k-1}{2} \right) - \Theta \left( \langle \sigma_i \rangle_{\beta_m, h} - \frac{2k+1}{2} \right) \right] \quad (9)$$

The function  $\Omega(\langle \sigma_i \rangle_{\beta_m, h})$  is shown in FIG. 1. A real number  $\langle \sigma_i \rangle_{\beta_m, h}$  is translated into the closest integer. Then we regard the above discrete value  $\Omega(\langle \sigma_i \rangle)$  as the value of  $i$ -th pixel for restored image at finite  $\beta_m$  and  $h$  in the finite temperature process.

In the MAP estimation, the estimation of the original image is regarded as the set  $\{\sigma_i\}$  which maximizes the posterior probability distribution (Eq.s (3),(6)). In other words, it is the set that minimizes the energy of the system described by the Hamiltonian  $\mathcal{H}_G$  or  $\mathcal{H}_B$  and is actually the ground state. Consequently, the above estimation corresponds to the MAP estimation when  $T_m \rightarrow 0$  ( $\beta_m \rightarrow \infty$ ) keeping  $H = h/\beta_m$  constant.

It is very important to evaluate the performance of restoration by means of these estimations. For this purpose, we assume that we know the original image and evaluate the performance of restoration by measuring the distance between the original and the restored images given by the above estimation. In order to measure the distance between the original and the restored images, we use the following mean square error as the distance,

$$H_D = \frac{1}{N} \sum_i [\xi_i - \Omega(\langle \sigma_i \rangle_{\beta_m, h})]^2, \quad (10)$$

whose value depends on the hyper-parameters  $h$  and  $\beta_m$  appearing in the thermal average.

### C. Method of threshold division

We next discuss the restoration of gray-scale image using bit-decomposed data. It is expected that the effects of noise on the binary data is lower than that on the  $Q$ -value data for image restoration: the binary data is estimated easily compared with the  $Q$ -value data because of the explicit representation. Since the original image is estimated by using the information of degraded image, the performance of restoration ought to be deeply affected by the effects of noise. Therefore we expect that the performance of restoration is improved by using the binary data instead of the  $Q$ -value data.

We generate binary data from  $Q$ -value data using the  $Q$ -Ising form by means of the following function

$$\Theta(\xi_i - k) = \xi_{i,k} = \begin{cases} 1 & (\xi_i \geq k) \\ 0 & (\xi_i < k), \end{cases} \quad (11)$$

where  $k$  ( $\in \{1, 2, \dots, Q-1\}$ ) is the threshold value and  $\xi_i$  ( $\in \{0, 1, \dots, Q-1\}$ ) is the input data. We can obtain  $(Q-1)$  sets of binary data from a  $Q$ -value data by using this function with threshold value changed from 1 to  $Q-1$ . This method is called the threshold division. For example, we consider a set with  $Q = 3$  (0, or 1, or 2) and six pixels:  $\{1, 2, 1, 1, 0, 2\}$ . If we insert this set into the above function with the threshold value  $k = 2$ , the binary set  $\{0, 1, 0, 0, 0, 1\}$  is generated. The set  $\{1, 1, 1, 1, 0, 1\}$  is also generated when  $k = 1$ . Thus two binary sets  $\{0, 1, 0, 0, 0, 1\}$  and  $\{1, 1, 1, 1, 0, 1\}$  are generated from the 3-value set  $\{1, 2, 1, 1, 0, 2\}$ . These operations are depicted in FIG. 2. The expression of binary data  $\xi_{i,k}$  ( $\in \{0, 1\}$ ) produced by this method is different from the usual binary notation because the relation between a  $Q$ -value data and  $(Q-1)$  sets of binary data becomes

$$\xi_i = \xi_{i,1} + \xi_{i,2} + \dots + \xi_{i,Q-1} = \sum_{k=1}^{Q-1} \xi_{i,k}. \quad (12)$$

We call binary data generated by this threshold division the bit-decomposed data (BDD).

Next, the process in the restoration of gray-scale image using the bit-decomposed data becomes the following.

1. Decompose a  $Q$ -value data (original image) into  $(Q-1)$  sets of binary data before transmission.
2. Send  $(Q-1)$  sets of binary data through a noisy channel.
3. Receive  $(Q-1)$  sets of corrupted binary data (degraded image).
4. Restore the original image from the degraded image.

This process is shown in FIG. 3. Obviously, this procedure is different from the method in which the raw  $Q$ -value data are sent.

Following the general formulation mentioned in the previous section, we formulate the above process. The posterior probability necessary for restoration is the following

$$\begin{aligned} P(\{\sigma\}|\{\tau_1\}, \{\tau_2\}, \dots, \{\tau_{Q-1}\}) &= \frac{P(\{\tau_1\}, \{\tau_2\}, \dots, \{\tau_{Q-1}\}|\{\sigma\})P_m(\{\sigma\})}{\text{tr}_{\{\sigma\}}P(\{\tau_1\}, \{\tau_2\}, \dots, \{\tau_{Q-1}\}|\{\sigma\})P_m(\{\sigma\})} \\ &\sim \prod_k^{Q-1} P_k(\{\tau_k\}|\{\sigma_k\})P(\{\sigma\}) \\ &\sim \exp \left( -h \sum_i \sum_k (\sigma_{i,k} - \tau_{i,k})^2 - \frac{\beta_m}{2z} \sum_{i,j} (\sigma_i - \sigma_j)^2 \right), \end{aligned} \quad (13)$$

where we used  $\{\sigma\}$  to denote the dynamical variables used to estimate  $\{\xi\}$ . The notation  $\sigma_{i,k} \in \{0, 1\}$  is the estimation of decomposed data  $\xi_{i,k}$ . The notation  $\tau_{i,k} \in \{0, 1\}$  is the degraded binary data. The relation between  $\sigma_{i,k}, \tau_{i,k}$  and  $\sigma_i, \tau_i$  is the same as that between  $\xi_i$  and  $\xi_{i,k}$  (Eq. (12)).

In the restoration of gray-scale image using the  $Q$ -Ising form, the posterior probability distribution is given by

$$P(\{\sigma\}|\{\tau\}) \sim \exp \left( -h \sum_i (\sigma_i - \tau_i)^2 - \frac{\beta_m}{2z} \sum_{ij} (\sigma_i - \sigma_j)^2 \right). \quad (14)$$

The difference of the posterior probability between our method (13) and the  $Q$ -Ising form (14) is only in the random field term. That is to say, the effects of noise in our method are different from the case where the raw  $Q$ -Ising data are sent.

### III. INFINITE-RANGE MODEL

In this section, we discuss the restoration of the gray-scale image in the infinite-range model. Since the infinite-range model is the model in which all pixels interact mutually, it is not useful for restoration of real images directly. However, the analysis of image restoration in the infinite-range model is very useful in understanding qualitatively the property of macroscopic quantities. In this section, we investigate both static and dynamical properties of macroscopic quantities in the infinite-range model. In the next subsection, we first calculate the free energy of system by means of the replica method and analyze the behavior of magnetization in the restored image and the mean square error for some ratio of the hyper-parameters. We compare the performance of restoration using our method and the  $Q$ -Ising form finally. We next clarify how the restored image reaches the equilibrium state and conditions that give the optimal restored image in section III B.

#### A. Static properties

Suppose that the prior probability generates the original image in the infinite-range model like Eq. (1). Then the  $i$ -th pixel interacts all other pixels and the prior probability distribution is represented as

$$P_s(\{\xi\}) = \frac{1}{Z(\beta_s)} \exp \left[ -\frac{\beta_s}{2N} \sum_{ij} (\xi_i - \xi_j)^2 \right], \quad (15)$$

where  $N$  is the system size and  $Z(\beta_s)$  is the partition function of the ferromagnetic  $Q$ -Ising model. We assume that the original image is generated by this probability both in the bit-decomposed data case and the  $Q$ -Ising case. In this section we adopt as the original image a snap shot of the system produced by the above probability.

We treat the Gaussian channel for simplicity. In our method, the Gaussian channel in which input data are expressed in a binary form is given by

$$P_k(\{\tau_{i,k}\}|\{\xi_{i,k}\}) = \frac{1}{\sqrt{2\pi}\tau} \exp \left[ -\frac{1}{2\tau^2} \sum_i (\tau_{i,k} - \tau_0 \xi_{i,k})^2 \right], \quad (16)$$

where  $\tau_{i,k}$  is a Gaussian random variable with mean  $\tau_0 \xi_{i,k}$  and variance  $\tau^2$ . The input  $\xi_{i,k}$  takes 0 or 1. For comparison, the  $Q$ -Ising case is denoted

$$P(\{\tau_i\}|\{\xi_i\}) = \frac{1}{\sqrt{2\pi}\tau'} \exp \left[ -\frac{1}{2\tau'^2} \sum_i (\tau_i - \tau'_0 \xi_i)^2 \right], \quad (17)$$

where  $\xi_i$  takes a value between 0 and  $Q - 1$ , and  $\tau_i$  is a Gaussian random variable with mean  $\tau'_0 \xi_i$  and variance  $\tau'^2$ . We calculate the posterior probability using Eq. (16) and Eq. (17).

In the bit-decomposed data case;

$$\begin{aligned} P(\{\sigma\}|\{\tau_1\}, \{\tau_2\}, \dots, \{\tau_{Q-1}\}) &\sim \prod_k^{Q-1} P_k(\{\tau_k\}|\{\sigma_k\}) P_m(\{\sigma\}) \\ &\sim \exp \left( -h \sum_i \sum_k (\sigma_{i,k} - \tau_{i,k})^2 - \frac{\beta_m}{2N} \sum_{i,j} (\sigma_i - \sigma_j)^2 \right) \\ &\equiv \exp(-H_{\text{eff}}). \end{aligned} \quad (18)$$

In the  $Q$ -Ising case;

$$P(\{\sigma\}|\{\tau\}) \sim \exp \left( -h \sum_i (\sigma_i - \tau_i)^2 - \frac{\beta_m}{2N} \sum_{i,j} (\sigma_i - \sigma_j)^2 \right). \quad (19)$$

The difference of these expressions and equations (13), (14) in previous section is only that the coordination number  $z$  became  $N$ .

We calculate the free energy from these probability distributions to clarify the behavior of macroscopic quantities. Since there is randomness in the field for the spin system described by the effective Hamiltonian  $H_{\text{eff}}$  in equations (18) and (19), the free energy must be averaged over the probability distribution of the random field in addition to the thermal average. More explicitly, supposing that the random variables  $\tau_i$  (or  $\tau_{i,k}$ ) and  $\xi_i$  (or  $\xi_{i,k}$ ) in the effective Hamiltonian  $H_{\text{eff}}$  are quenched, we first average with respect to the degree of freedom of the spin  $\sigma$  and get the free energy of usual statistical mechanics. Afterwards, the free energy is averaged over the probability distributions of  $\tau_i$  (or  $\tau_{i,k}$ ) and  $\xi_i$  (or  $\xi_{i,k}$ ). The latter is called the configurational average, which is expressed by  $[\dots]$  in this section. Accordingly, we calculate the free energy per site by

$$f = F/N = -\frac{1}{N\beta_m} [\ln Z]. \quad (20)$$

Calculation of the configurational average  $[\ln Z]$  is, however, not easy because the dependence of logarithm of the partition function on the quenched random variables is very complicated. Therefore, we use an identity

$$[\log Z] = \lim_{n \rightarrow 0} \frac{[Z^n] - 1}{n}. \quad (21)$$

By this equation, we calculate not  $[\ln Z]$  but  $[Z^n]$  and take the limit  $n \rightarrow 0$ . The calculation of  $[Z^n]$  is easier than that of  $[\ln Z]$ . This method is called the replica method [13]. We must evaluate the following

average of the replicated partition function,

$$\begin{aligned}
[Z^n] &= \sum_{\xi} \sum_{\tau} P_s(\{\xi\}) P(\{\tau\} | \{\xi\}) \text{Tr}_{\sigma} e^{-H_{\text{eff}}^{\text{rep}}} \\
&= \text{Tr}_{\xi} \int \prod_{i,k} d\tau_i^{(k)} \frac{1}{(\sqrt{2\pi}\tau)^{(Q-1)N}} \exp\left[-\frac{1}{2\tau^2} \sum_i (\tau_i - \tau_0 \xi_i)^2\right] \times \exp\left[-\frac{\beta_s}{2N} \sum_{ij} (\xi_i - \xi_j)^2\right] \\
&\quad \times \text{Tr}_{\sigma} \exp\left[-h \sum_i \sum_k \sum_{\alpha} (\tau_{i,k} - \sigma_{i,k}^{\alpha})^2 - \frac{\beta_m}{2N} \sum_{ij} \sum_{\alpha} (\sigma_i^{\alpha} - \sigma_j^{\alpha})^2\right], \tag{22}
\end{aligned}$$

where  $\alpha$  is the label of  $n$  dummy replicas. Assuming replica symmetric ansatz  $m_{\alpha} = m$  ( $\forall \alpha$ ), the following expressions of the order parameters are derived.

$$[\xi_i] = m_0 = \frac{1}{Z(\beta_s)} \text{tr}_{\xi} \xi e^{2m_0 \beta_s \xi - \beta_s \xi^2}, \tag{23}$$

$$[\langle \sigma_i^{\alpha} \rangle] = m = \frac{1}{Z(\beta_s)} \text{tr}_{\xi} \xi e^{2m_0 \beta_s \xi - \beta_s \xi^2} \int Du_1 \cdots \int Du_{Q-1} \frac{\text{tr}_{\sigma} \sigma \exp(\tilde{H}_{\text{eff}})}{\text{tr}_{\sigma} \exp(\tilde{H}_{\text{eff}})}, \tag{24}$$

where

$$Du \equiv \frac{du}{\sqrt{2\pi}} e^{-u^2/2}, \tag{25}$$

$$\tilde{H}_{\text{eff}} \equiv 2\beta_m m \sigma - \beta_m \sigma^2 - h \sum_k \sigma_k^2 + 2h\tau \sum_k u_k \sigma_k + 2h\tau_0 \sum_k \xi_k \sigma_k. \tag{26}$$

The derivation of equations (23) and (24) is given in Appendix A. Equation (23) represents the magnetization of the original image in the infinite range model. The behavior of the source magnetization  $m_0$  as a function of the temperature  $\beta_s$  is shown in FIG. 4. Equation (24) is the equation of state for the magnetization of the restored image. In the limit  $N \rightarrow \infty$ , the mean square error (Eq. (10)) is rewritten as

$$H_D = \frac{1}{Z(\beta_s)} \text{tr}_{\xi} \xi e^{2m_0 \beta_s \xi - \beta_s \xi^2} \int Du_1 \cdots \int Du_{Q-1} \{ \xi_i - \Omega(\langle \sigma_i^{\alpha} \rangle) \}^2. \tag{27}$$

We next assume a condition to compare the performance of restoration between using the bit-decomposed data and the  $Q$ -Ising form. The condition is that the distance between the original and the degraded images in our method is equal to that in the  $Q$ -Ising form. We can compare the difference of performance in disparate noisy channels by this condition. The distance between the original and degraded images in our method  $H_D^{\tau}$ (BDD) is expressed similarly to the above expression. It turns out that the distance  $H_D^{\tau}$ (BDD) becomes simple in the thermodynamic limit  $N \rightarrow \infty$ .

$$\begin{aligned}
H_D^{\tau}(\text{BDD}) &= \frac{1}{N} \sum_i \{ (\xi_{i,1} + \xi_{i,2} + \cdots + \xi_{i,Q-1}) - (\tau_{i,1} + \tau_{i,2} + \cdots + \tau_{i,Q-1}) \}^2 \\
&= \left\langle \left( \sum_k \xi_k - \sum_k \tau_k \right)^2 \right\rangle_{\tau_1, \dots, \tau_{Q-1}, \xi_1 \dots \xi_{Q-1}} \\
&= (Q-1)\tau^2 + \frac{(\tau_0 - 1)^2}{Z(\beta_s)} \text{tr}_{\xi_1 \dots \xi_{Q-1}} \left[ \sum_{k=1}^{Q-1} \xi_k e^{2\beta_s m_0 \sum_k \xi_k - \beta_s (\sum_k \xi_k)^2} \right] \\
&= (Q-1)\tau^2. \tag{28}
\end{aligned}$$

When the mean  $\tau_0$  of the Gaussian noise is 1, the distance  $H_D^{\tau}$ (BDD) depends on the variance  $\tau^2$  only. In the  $Q$ -Ising form,  $H_D^{\tau}$ ( $Q$ -Ising) is

$$H_D^{\tau}(\text{Q-Ising}) = \frac{1}{N} \sum_i \{ \xi_i - \tau_i \}^2$$

$$\begin{aligned}
&= \tau'^2 + \frac{(\tau'_0 - 1)^2}{Z(\beta_s)} \text{tr}_\xi \left[ \xi e^{2\beta_s m_0 \xi - \beta_s \xi^2} \right] \\
&= \tau'^2
\end{aligned} \tag{29}$$

where  $\tau'^2$  is the variance of a Gaussian channel in the  $Q$ -Ising form and is different from  $\tau$  in the bit-decomposed data. When  $\tau'_0 = 0$ ,  $H_D^\tau(Q\text{-Ising}) = \tau'^2$  similarly to the bit-decomposed data case. As the rate of degradation is equal to each other, namely  $H_D^\tau(\text{BDD}) = H_D^\tau(Q\text{-Ising})$ , the variance of a noisy channel between our method (28) and that in the  $Q$ -Ising form (29) satisfies the following relation.

$$\tau = \frac{\tau'}{\sqrt{Q-1}} \tag{30}$$

Next, we calculate the restoration of gray-scale image when  $Q = 3$ . We plot the magnetization  $m_0$  of original image as a function of source temperature  $T_s$  for  $Q = 3$  in FIG. 4. In high temperature region  $T_s \rightarrow \infty$ , the magnetization becomes  $m_0 = (0 + 1 + 2)/3 = 1$  since each spin takes all the values with the same probability 1/3. We see that two locally stable states are generated in the middle range of temperature. The globally stable state is the line of  $m_0 = 1$ . The transition temperature between the paramagnetic phase and the ferromagnetic phase is  $T_c \sim 0.9$ . These locally stable states become more stable with the decrease of temperature and correspond to the globally stable states  $m_0 = 0$  and  $m_0 = 2$  in  $T_s = 0$ . That is, the system of the ferromagnetic  $Q$ -Ising model for  $Q = 3$  has triple degeneracy.

We use a snapshot of the system when the magnetization is  $m_0 = 1$  at  $T_s = 0.75$  as the original image. When the distance between the original image and the degraded image is  $H_D^\tau = 1.0$ , macroscopic quantities behave as in FIG. 5. The magnetization  $m$  of equation (24) at the ratio of hyper-parameters  $H \equiv h/\beta_m = 0.25$  has three stable states at  $T_m = 0$  as  $m_0$  we see in the original image. At low temperature, the system has one globally stable state  $m = 1$  and two locally stable states  $m = 0$  and  $m = 2$ . However these locally stable states vanish as the ratio of hyper-parameters  $H$  becomes large. Seeing the free energy in FIG. 5, we find that the state of system branches out into a global minimum and local minima at  $T_m = 0.27$ .

The mean square error  $H_D$  using  $m$  of the global minimum is smaller than that using  $m$  of local minimum in all temperature region and gives the optimal value for the ratio of hyper-parameters  $H$ . The mean square error  $H_D$  between the  $m$  of global minimum and the original image  $m_0$  in some ratio of hyper-parameters  $H$  are described in figure 6. The smallest mean square error is given at  $T_m = 0.75$  and  $H = 0.75$ . When the distance between the original and degraded images is 1.0 ( $H_D^\tau = 1.0$ ), we see that the deviation  $\tau$  of Gaussian noise becomes  $1/\sqrt{Q-1} = 1/\sqrt{2}$  by equation (28). Therefore, when the ratio of hyper-parameters corresponds to that of the prior parameters ( $H = h/\beta_m = (\tau_0/2\tau^2)/\beta_s = 0.75$ ), the optimal restoration is given at the temperature corresponding to the source temperature ( $T_m = T_s = 0.75$ ) similarly to the Ising model. At high temperatures  $T_m \rightarrow \infty$ , all states appear with equal probability. Then the thermal average of a spin  $\sigma$  becomes  $\langle \sigma \rangle = (0 + 1 + 2)/3 = 1$  at all pixels. The mean square error is

$$H_D(T_m \rightarrow \infty) = \frac{\sum_{\xi=0}^3 (\xi - 1)^2 e^{2m_0 \beta_s \xi - \beta_s \xi^2}}{\sum_{\xi=0}^3 e^{2m_0 \beta_s \xi - \beta_s \xi^2}} \sim 0.3452. \tag{31}$$

If the distance between the original and degraded images,  $H_D^\tau(\text{BDD})$  or  $H_D^\tau(Q\text{-Ising})$ , is extremely large, the performance of restoration does not become smaller than this value.

We compare the optimal performance of restoration using our method with that using the  $Q$ -Ising form under the condition that the degradation of image in our method is equivalent to the one in the  $Q$ -Ising form, namely  $H_D^\tau(\text{BDD}) = H_D^\tau(Q\text{-Ising form})$ . In the  $Q$ -Ising form case, the deviation is  $\tau = 1.0$  by equation (29) when  $H_D^\tau = 1.0$ . The optimal restoration in the  $Q$ -Ising form is also given in the ratio of hyper-parameters corresponding to that of source parameters ( $H = h/\beta_m = (\tau_0/2\tau^2)/\beta_m = 0.375$ ). The optimal performance of restoration in both our method and the  $Q$ -Ising form is shown in FIG. 6. We see that the restoration by our method gives better performance than that of the  $Q$ -Ising form.

## B. Dynamical properties

In the previous section, we investigated the static properties of image restoration within the framework of equilibrium statistical mechanics. However, we do not understand how restored image reaches the equilibrium state at each temperature. In this section, we discuss the dynamical properties of image restoration in the infinite-range model and investigate some conditions to get the restored image which is more similar to the original image than the given degraded image.

There are a lot of local stable states for the spin system described by the effective Hamiltonian  $H_{\text{eff}}$  because of the random field. In addition, the number of local minima increases with the gray-scale level, namely  $Q$ -state values. If the system is attracted to such local minima in the restoration process, it is possible that the restored image is different from the original image. Since the final state of the restoration process depends on the initial condition of the spin system as well as on the hyper-parameters  $h$  and  $\beta_m$ , it is important to investigate the dynamics of the macroscopic variables  $m$  and  $H_{\text{D}}$ . Therefore, we derive the time-dependent equation of magnetization from the master equation of our system and investigate the dynamics of the mean square error by means of the equation of magnetization.

The master equation of our system is written as

$$\frac{dp_t(\boldsymbol{\sigma})}{dt} = \sum_{k=1}^N \sum_{\sigma_{k'}=0}^{Q-1} [\omega(\sigma_{k'} \rightarrow \sigma_k) p_t(\boldsymbol{\sigma}') - \omega(\sigma_k \rightarrow \sigma_{k'}) p_t(\boldsymbol{\sigma})], \quad (32)$$

where  $p_t(\boldsymbol{\sigma})$  is the probability that the system is in a certain state  $\boldsymbol{\sigma}$ . Those states are defined as  $\boldsymbol{\sigma} \equiv (\sigma_1, \dots, \sigma_k, \dots, \sigma_N)$  and  $\boldsymbol{\sigma}' \equiv (\sigma_1, \dots, \sigma_{k'}, \dots, \sigma_N)$ . The difference between  $\boldsymbol{\sigma}$  and  $\boldsymbol{\sigma}'$  is only spin in the  $k$ th site. The transition probability  $\omega(\sigma_k \rightarrow \sigma_{k'})$  is given by

$$\omega(\sigma_k \rightarrow \sigma_{k'}) = \frac{\exp[-\Delta E]}{\text{tr}_{\sigma_{k'}^{(1)}, \dots, \sigma_{k'}^{(Q-1)}} \exp[-\Delta E]} = \frac{\exp[h_{\text{eff}}]}{\text{tr}_{\sigma_{k'}^{(1)}, \dots, \sigma_{k'}^{(Q-1)}} \exp[h_{\text{eff}}]}, \quad (33)$$

where

$$h_{\text{eff}} = -\beta_m (\sigma_{k'}^{(1)} + \dots + \sigma_{k'}^{(Q-1)})^2 - h (\sigma_{k'}^{(1)} + \dots + \sigma_{k'}^{(Q-1)})^2 + \sum_{l=1}^{Q-1} (2\beta_m + 2h\tau_{k'}) \sigma_{k'}^{(l)}. \quad (34)$$

Furthermore, the probability that the macroscopic magnetization is  $m$  at time  $t$  is defined as

$$\mathcal{P}_t(m) \equiv \sum_{\boldsymbol{\sigma}} p_t(\boldsymbol{\sigma}) \delta[m - m(\boldsymbol{\sigma})], \quad (35)$$

Substituting Eq. (32) into this expression, we obtain the time-dependent equation of magnetization as

$$\frac{dm}{dt} = -m(t) + \frac{\text{tr}_{\xi} e^{2\beta_s m_0 \xi - \beta_s \xi^2}}{Z(\beta_s)} \int Du_1 \dots \int Du_{Q-1} \frac{\text{tr}_{\sigma} \sigma e^{H_{\text{eff}}}}{\text{tr}_{\sigma} e^{H_{\text{eff}}}} \quad (36)$$

where  $H_{\text{eff}}$  is the same as in the static case. The derivation of equation (36) is given in Appendix B. The dynamics of the mean square error  $H_{\text{D}}(t)$  is obtained by substituting the time-dependent expression of magnetization (36) into the static expression of mean square error  $H_{\text{D}}(m)$ .

We now show the results of equation (36) for the prior parameter conditions:  $Q = 3$ ,  $T_s = 0.75$ ,  $m_0 = 1.0$ ,  $\tau_0 = 1.0$ ,  $\tau = 1/\sqrt{2}$ . The time evolution of magnetization  $m(t)$  and mean square error  $H_{\text{D}}(t)$  when hyper-parameters corresponds to the prior parameters ( $T_m = T_s$ ,  $H = h/\beta_m = (\tau_0/2\tau^2)/\beta_s$ ) are shown in the upper two figures of FIG. 7. We see that the state of the system converges at a macroscopic stable state for any initial state. The mean square error also converges to the same value and has the optimal value which is smaller than  $H_{\text{D}}^*$ . Basically, if we choose these values of hyper-parameters, we necessarily obtain the restored image closer to the original image than the degraded image without depending upon the initial image of restoration.

Next, we consider the results when the hyper-parameters are different from the prior parameters ( $T_m \neq T_s$ , or  $H = h/\beta_m \neq (\tau_0/2\tau^2)/\beta_s$ ). In this case, it is possible that there are locally stable

states as we see in the lower two figures of FIG. 7. The state of the system is attracted to a closer stable state depending on the initial state. The mean square error approaches the value corresponding to each stable state depending on the initial state. There is a threshold of initial value of mean square error:  $H_D^{(c)}$ . Beyond this threshold value  $H_D^{(c)}$ , the mean square error never converges to its optimal value. There is the threshold distance  $H_D^{(c)}$  between 0.75 and 0.95. The distance  $H_D^r$  between the original and the degraded images is 1.0 and it is larger than this threshold distance  $H_D^{(c)}$ . In this case, if we choose the degraded image as the initial image of restoration, the restored image is different from the original image entirely.

Next, we consider the relaxation time by which the system arrives at the equilibrium state at each temperature. The limiting value of magnetization  $m(t)$  as  $t \rightarrow \infty$  corresponds to the magnetization obtained by the static analysis, namely a solution of the saddle point equation (24). Then we define the asymptotic expression of the magnetization in the limit  $t \rightarrow \infty$  as follows

$$m(t) = \tilde{m} + ae^{-\frac{t}{t_0}}, \quad (37)$$

where  $\tilde{m}$  is a magnetization of the saddle point equation in the static case. Here, the coefficient  $a$  is defined by the constant  $m(t=0) - \tilde{m}$ .  $t_0$  is the relaxation time, which is expressed as follows,

$$t_0^{-1} = 1 - \frac{2\beta_m}{Z_s} \text{tr}_\xi e^{2\beta_s m_0 \xi - \beta_s \xi^2} \int Du_1 \cdots \int Du_{Q-1} \{ \langle \sigma^2 \rangle_{\tilde{H}_{\text{eff}}} - \langle \sigma \rangle_{\tilde{H}_{\text{eff}}}^2 \}. \quad (38)$$

Furthermore, the asymptotic expression of the mean square error by means of Eq. (37) becomes

$$H_D = H_D(\tilde{m}) + be^{-\frac{t}{t_0}}, \quad (39)$$

where

$$\begin{aligned} b = & 4\beta_m a e^{-\frac{t}{t_0}} \frac{1}{Z_s} \text{tr}_\xi e^{2\beta_s m_0 \xi - \beta_s \xi^2} \int Du_1 \cdots \int Du_{Q-1} \\ & [\xi - \Omega(\langle \sigma \rangle_{\tilde{H}_{\text{eff}}})] \times [\langle \sigma^2 \rangle_{\tilde{H}_{\text{eff}}} - \langle \sigma \rangle_{\tilde{H}_{\text{eff}}}^2] \\ & \times \sum_{k=1}^Q k \left[ \delta \left( \langle \sigma \rangle_{\tilde{H}_{\text{eff}}} - \frac{2k-1}{2} \right) + \delta \left( \langle \sigma \rangle_{\tilde{H}_{\text{eff}}} - \frac{2k+1}{2} \right) \right]. \end{aligned} \quad (40)$$

The derivations of the equations (38), (39) and (40) are given in Appendix C.

We calculate the inverse relaxation time  $t_0^{-1}$  as a function of temperature. For  $Q = 3$ ,  $T_s = 0.75$ ,  $\tau_0 = 1.0$ ,  $\tau = 1/\sqrt{2}$ , the inverse relaxation time in some ratio of hyper-parameters  $H$  is plotted in FIG. 8. The inverse relaxation time does not reach 0 and has always a finite value for all temperatures. Accordingly, the state of the system relaxes, exponentially, to the equilibrium state at finite temperatures.

#### IV. MONTE CARLO SIMULATION

In this section, we investigate realistic pictures in two dimensions and check the results obtained in the infinite-range model. It is, however, difficult to investigate the restoration of real images by analytical methods. We discuss the restoration of two-dimensional images by means of Monte Carlo simulations.

We suppose that the original image is generated by the Boltzmann probability distribution as we did in the infinite-range model case and we use a snap shot of the  $Q$ -Ising model at a temperature as the original image. In the cases of  $Q = 4$  and  $Q = 8$ , the magnetization of original image as a function of source temperature is plotted in FIG. 9. There are transition temperatures at which local minima are generated. The transition temperatures for  $Q = 4$  and  $Q = 8$  are about 0.38 and 1.0 respectively. It is important for image restoration whether the temperature at which the original image is generated is higher or lower than these transition temperatures. In image restoration, it is generally the case that an original image generated at lower temperature gives better performance of restoration. However, there is another important issue of the estimation of hyper-parameters. According to Iba, the hyper-parameters is estimated most reliably around the transition temperature in the Ising model [23, 24].

In digital images, the pixel takes discrete values. Even if real-valued Gaussian noise is added in the degradation process, we have to regard such a noise as the discrete noise (for example, binary noise) when both the original and the degraded images are digital. (This is essentially the same situation as in a error-correcting codes. [25]) Therefore, we consider the binary noise caused by the binary symmetric channel with the error probabilities  $p = 0.10$  ( $Q = 4$ ) and  $p = 0.15$  ( $Q = 8$ ), which correspond to the parameters  $\beta_\tau \sim 2.2$  and  $\beta_\tau \sim 1.7$  by Eq. (5). The size of digital image is  $100 \times 100$  and averages over ten samples are taken at each data point.

FIG. 10 (the upper figure) represents the mean square error of several  $H$  when  $Q = 4$ ,  $T_s = 0.35$ ,  $m_0 \sim 1.2$ ,  $p = 0.10$  and  $H_D^T \sim 0.30$ . The optimal restoration is given at  $T_m = T_s$ ,  $H = h/\beta_m = \beta_\tau/\beta_s \sim 0.75$  like in the infinite-range model.

The mean square errors for  $Q = 8$ ,  $T_s = 0.4$ , (0.6),  $m_0 \sim 2.2$ , (3.0),  $p = 0.15$ ,  $H_D^T \sim 1.0$  are also shown in FIG. 10 (the lower two figures). We see that the best performance of restoration at each temperature is obtained at the ratio of hyper-parameters  $H$  corresponding to that of the prior parameters, and the performance of restoration in  $T_s = 0.4$  is better than that in  $T_s = 0.6$  as written before.

## V. MEAN-FIELD ANNEALING

The amount of computation required for restoration by means of Monte Carlo simulation is enormous. Hence, in the present section, we reconstruct the original image from binary degraded images by means of the mean-field annealing [26, 27] with periodic boundary conditions. This method enables us to search for the optimal solution quickly. We apply the mean-field approximation to the posterior probability distribution.

$$P(\{\sigma\}|\{\tau_1\}, \{\tau_2\}, \dots, \{\tau_{Q-1}\}) = \frac{1}{Z(\beta_m, h)} \exp \left( -h \sum_i \sum_k (\sigma_{i,k} - \tau_{i,k})^2 - \frac{\beta_m}{2N} \sum_{i,j} (\sigma_i - \sigma_j)^2 \right) \quad (41)$$

In order to treat each site separately, we trace out with respect to all pixels besides  $i$ -th pixel in the above probability distribution.

$$\begin{aligned} \rho_{ij}(n) &= \prod_{kl \neq ij} \text{tr}_{\sigma_1, \dots, \sigma_{Q-1}} P(\{\sigma\}|\{\tau_1\}, \{\tau_2\}, \dots, \{\tau_{Q-1}\}) \\ &= \text{Tr}_{\sigma_1, \dots, \sigma_{Q-1}} P(\{\sigma\}|\{\tau_1\}, \{\tau_2\}, \dots, \{\tau_{Q-1}\}) \delta(n, \sigma_{ij}) \end{aligned} \quad (42)$$

where  $(ij)$  represents the site index in two dimensions:  $i$  and  $j$  are the coordinates of  $x$  and  $y$  axes, respectively. This expression is called the marginal probability distribution. According to mean-field approximation, the posterior probability distribution (41) is approximated by the product of the marginal probability distribution (42) as follows.

$$P(\{\sigma\}|\{\tau_1\}, \{\tau_2\}, \dots, \{\tau_{Q-1}\}) \simeq \prod_{(ij)} \rho_{ij}(n). \quad (43)$$

The recursion relation for the iterative algorithm is derived from a variational principle. To derive the recursion relation, we substitute the expression of approximation (43) to the free energy.

$$F(\rho) = E(\rho) - T_m S(\rho). \quad (44)$$

The variation of the above free energy is calculated with respect to the marginal probability distribution at a certain site:  $\rho_{ij}$ . Finally, the recursion relation with respect to the local magnetization for the iteration algorithm is obtained as

$$m_{ij}^{t+1} = \frac{\sum_{\sigma_{ij}=0}^{Q-1} \sigma_{ij} \exp(H_{\text{MF}}^t)}{Z_{\text{MF}}}, \quad (45)$$

$$\begin{aligned}
H_{\text{MF}}^t = & \frac{\beta_m}{2} (m_{i,j+1}^t + m_{i,j-1}^t + m_{i+1,j}^t + m_{i-1,j}^t) \sigma_{ij} \\
& - \beta_m \sigma_{ij}^2 - h \sum_k (\sigma_{ij,(k)})^2 + 2h \sum_k \tau_{ij,(k)} \sigma_{ij,(k)},
\end{aligned} \tag{46}$$

where  $Z_{\text{MF}}$  is the normalization constant in the mean-field approximation (see Appendix D for details of derivation).

We solve the above relations numerically under the convergence condition

$$\epsilon^{(t)} \equiv \frac{1}{N} \sum_{(ij)}^N |m_{ij}^{(t+1)} - m_{ij}^{(t)}| < 10^{-8}, \tag{47}$$

and obtain approximately the restored image at each temperature. The annealing schedule is set at  $\Delta T_m = 0.01$ .

We compare the performance of restoration using our method with that using the  $Q$ -Ising form for five kinds of standard images [28]. We choose  $Q = 8$ , system size =  $200 \times 200$  and  $H_D^T \simeq 1.00$ . The result is shown in table I. The original versions of these five standard image are shown in FIG. 11.

The original, degraded and optimal restored images in our method and  $Q$ -Ising form are shown in FIG. 12 ("lena") for the case of "lena".

In TABLE I, the ratio of pixels at which the nearest neighboring pixels take the same value is also represented. We see that the performance of restoration using our method is better than that using the  $Q$ -Ising form in the standard pictures "chair" and "girl". But, the  $Q$ -Ising form is better in "house", "lena" and "mant". One of the differences is that "chair" and "girl" have a lot of large parts and do not have short edges compared with the other pictures as we see intuitively. In TABLE I, that "chair" has obviously large parts is quantitatively expressed by the ratio of pixels at which the nearest neighboring pixels take the same value. However, the ratio in "girl" is as much as that in "house" and "lena".

In order to investigate this aspect in more detail, we show the ratio of pixels at which the difference among the value of the nearest neighboring pixels is smaller than 2 in table II. As seen in TABLE II, "girl" is similar to "chair" rather than "house" and "lena". The effects of noise in the bit-decomposed data and  $Q$ -Ising form are clarified by comparing the NNP1-D in TABLE I and NNP2-D in TABLE II. NNP1-D in our method is smaller than that in the  $Q$ -Ising form for all kinds of standard images, but the decrease of NNP2 from the original image to the degraded image in our method is small compared with that in the  $Q$ -Ising form for five standard images. That is, the noise in our method affects the original image widely, but the shift of value in a site is small. On the other hand the shift of value in a site is large in the  $Q$ -Ising form. Therefore the noise in our method has the effect of smoothing, and the restoration using our method is efficient for original images in which eliminating noise is more significant than preserving informations of original image as "chair" and "girl".

Furthermore, we compare the performance using our method and in the  $Q$ -Ising form for the  $H_D^T \sim 2.0$  case. Other conditions are the same as the previous case. We can simply investigate the tolerance of our method and  $Q$ -Ising form against noise by comparing  $H_D^T \sim 1.0$  and  $2.0$  cases. The performance of restoration is shown in TABLE III and the resultant image is presented in FIG. 13 for the case of "lena". The performance of restoration is clearly worse than that in the previous case for all pictures, and the difference of performance between our method and the  $Q$ -Ising form is clear. Moreover, the restoration using our method gives better performance than that using the  $Q$ -Ising form in standard image "house". The result is different from that when  $H_D^T \sim 1.0$ . In the  $Q$ -Ising form, large clusters remain in the restored image as in FIG. 13. Accordingly we conclude that the restoration using the bit-decomposed data is not affected by the noise compared with that using the  $Q$ -Ising form in this case.

Consequently we found that the restoration using our method is more efficient than that in the  $Q$ -Ising form in original images where the nearest neighboring pixels take the close values. The reason is that to eliminate the added noise is more significant than the information of the original image in such images. Regardless of the  $Q$ -Ising form and our method, the restoration of such images tend to give good performance compared with that of other images in the image restoration using the method of statistical mechanics. Moreover, our method can give the adequate restored image in original images "chair", "girl" and "house" even if the noise is strong to a certain extent: for example,  $H_D^T \sim 2.0$ .

Finally, we try to restore the original image by using the composition of our method and the  $Q$ -Ising form. Two processes are considered in restoration using the composition. One is the method of restoration

where the original image is restored from  $Q - 1$  sets of binary degraded images which are generated from the received, degraded  $Q$ -value image by the method of threshold division. Another is the method of restoration where the original image is restored by using the  $Q$ -Ising form after translating  $Q - 1$  sets of binary degraded images into a  $Q$ -value degraded image. These restoration processes are shown in FIG. 14.

The second process is not efficient in the restoration of gray-scale image because the performance of restoration is worse than that both using our method and the  $Q$ -Ising form. On the other hand, the first process gives interesting results as in TABLE IV when  $H_D^\tau \sim 1.0$ . Seeing in TABLE IV, we find that this method gives better performance than our method and the  $Q$ -Ising form for all standard images: "chair", "girl", "house", "lena" and "mant". The restoration of standard images using this method for the case of "lena" is shown in FIG. 15. This idea that, after a  $Q$ -value data are received, they are decomposed into binary data has been already used in the field of engineering. The filter is called the Stack filter which works on decomposed binary data after reception.

The Stack filter by means of the method of statistical mechanics as the first process gives better performance than the other two methods, but the theoretical framework is not clear. Because we have to assume the noisy process matching the degraded data in the Bayesian viewpoint, it is very difficult for us to estimate the noisy channel matching such binary data. Accordingly, it is well possible that the hyper-parameter  $h$  can not be estimated appropriately for the hyper-parameters estimation in the Stack filter by means of the method of statistical mechanics.

## VI. SUMMARY AND DISCUSSIONS

In this paper, we investigated the restoration of gray-scale image using the bit-decomposed data instead of the conventional  $Q$ -Ising form and found the conditions that our method is more efficient than the method of the  $Q$ -Ising form.

In the infinite-range model, we analyzed the image restoration when the original image is affected by the Gaussian noise, and obtained the static and dynamical properties of image restoration. In order to get the static properties, we calculated the restoration of gray-scale image by means of the replica method. Then we found that the mean square error has a minimum at the finite temperature for any ratio of the hyper-parameters  $H$ . However, when the noise rate is extremely large, the minimum sinks under the mean square error  $H_D(T_m \rightarrow \infty)$  in the high temperature limit. In other words, we can only obtain the restored image in which all states appear with equal probability as the optimal restored image when the original image is very corrupted. The best performance of restoration is given at the temperature at which the original image is generated, when the ratio of hyper-parameters corresponds to that of the prior parameters. This result is also common between the Ising spin and the  $Q$ -Ising spin cases. Furthermore, we obtained the quantitative result that the performance of restoration using our method is better than that using the  $Q$ -Ising form when  $H_D^\tau(\text{BDD}) = H_D^\tau(\text{Q-Ising})$ .

In order to get the dynamical properties of gray-scale image restoration, we derived the time-dependent equations of macroscopic quantities from the master equation. We found that, if we choose the hyper-parameters appropriately, the mean square error converges to the optimal value from any initial state of restoration. On the other hand, if we fail to set the hyper-parameters appropriately, the mean square error converges to a wrong value. In this case, even if we choose the degraded image as the initial state of restoration, the obtained restored image is worse than the degraded image and is different from the original image clearly. However, since we do not generally know the actual values of hyper-parameters, we need to estimate the hyper-parameters. This estimation of the hyper-parameters is also an important problem and is investigated by many people [23, 24, 29, 30, 31]. But, we do not discuss the estimation of hyper-parameters in this thesis.

We analyzed the restoration of realistic images in two dimensions by means of Monte Carlo method and the mean-field annealing approximately. Using Monte Carlo method, we confirmed the result of the infinite-range model that the mean square error gives the optimal minimum value at the temperature corresponding to the source temperature when the ratio of hyper-parameters corresponds to prior parameters for a snap-shot of the  $Q$ -Ising model for  $Q = 4$  and  $Q = 8$ . We restored five standard images by means of the mean-field annealing and found that the restoration using our method is better than that using the  $Q$ -Ising form in the original images where keeping the information of original image is not significant compared with the eliminating the added noise as "chair" and "girl". The reason is that the

effects of noise in our method contain the effect of smoothing. However, our method is not efficient in images which need information of the original image strongly.

Thus there are simply two types in natural images. One is the image which consists of a little long edges and large surfaces, and those images depend on a basic and common property of natural image strongly. Another is the image which has many short edges and small clusters, and it is difficult to distinguish whether the original or degraded images in such images. Therefore not only corrupted parts but correct parts may be destroyed by the effect of smoothing in such images. In restoration of images by means of the method of statistical mechanics, the effect of smoothing is strong compared with keeping the information of original image that the degraded image contains because we use it as common property of natural images. Therefore, we need some additional information on the original image.

Furthermore, we found also that the restoration using our method is not affected by noise compared with that using the  $Q$ -Ising form. One of the reasons is due to that the output, namely the degraded data, takes the close value to input data by the effects of noise in our method. This is the most significant property of our method. We expect that the restoration using our method gives further better performance when  $Q$ -value is large. Because we could not distinguish visually the difference between close values with increasing the gray-scale level ( $Q$ -value), the effect of noise may be suppressed visually. Accordingly, we may obtain the restored image that looks closer to the original image intuitively.

The authors thank Professor Hidetoshi Nishimori for useful discussions in this study.

## APPENDIX A: STATIC PROPERTIES OF THE INFINITE-RANGE MODEL

In this appendix, we calculate equation (22) by means of the replica trick and derive equations of state (23) and (24).

We define the replicated Hamiltonian  $H_{\text{eff}}^{\text{rep}}$  as

$$H_{\text{eff}}^{\text{rep}} \equiv H_{\text{F}}^{\text{rep}} + H_{\text{R}}^{\text{rep}}, \quad (\text{A1})$$

where the ferromagnetic term and the random field term are, respectively, expressed by

$$\begin{aligned} H_{\text{F}}^{\text{rep}} &= \frac{\beta_m}{2N} \sum_{ij} \sum_{\alpha} (\sigma_i^{\alpha} - \sigma_j^{\alpha})^2 \\ &= \beta_m \sum_i \sum_{\alpha} (\sigma_i^{\alpha})^2 - \frac{\beta_m}{N} \sum_{ij} \sum_{\alpha} \sigma_i^{\alpha} \sigma_j^{\alpha} \\ &= \beta_m \sum_i \sum_{\alpha} (\sigma_i^{\alpha})^2 - \frac{\beta_m}{N} \sum_{\alpha} (\sum_i \sigma_i^{\alpha})^2, \end{aligned} \quad (\text{A2})$$

$$\begin{aligned} H_{\text{R}}^{\text{rep}} &= h \sum_i \sum_k \sum_{\alpha} (\tau_{i,k} - \sigma_{i,k}^{\alpha})^2 \\ &= h \sum_i \sum_k \sum_{\alpha} (\sigma_{i,k}^{\alpha})^2 - 2h \sum_i \sum_k \sum_{\alpha} \tau_{i,k} \sigma_{i,k}^{\alpha} \\ &\quad + nh \sum_i \sum_k (\tau_{i,k})^2. \end{aligned} \quad (\text{A3})$$

The third term in the random field term vanishes in the limit  $n \rightarrow 0$ . The second term is related to the average over the probability distribution of  $\tau_{i,k}$ . The average over the probability distribution  $P(\{\tau\}|\{\xi\})$  leads to

$$\begin{aligned} &\sum_{\tau} P(\{\tau\}|\{\xi\}) \text{tr}_{\sigma} e^{-H_{\text{R}}^{\text{rep}}} \\ &= \int_{-\infty}^{\infty} \prod_{i,k} d\tau_{i,k} \frac{1}{(\sqrt{2\pi}\tau)^{(Q-1)N}} \\ &\quad \times \text{tr}_{\sigma} \exp \left[ -\frac{1}{2\tau^2} \sum_i (\tau_i - \tau_0 \xi_i)^2 - h \sum_i \sum_k \sum_{\alpha} (\sigma_{i,k}^{\alpha})^2 + 2h \sum_i \sum_k \sum_{\alpha} \tau_{i,k} \sigma_{i,k}^{\alpha} \right] \\ &= \text{tr}_{\sigma} \exp \left[ -h \sum_i \sum_k \sum_{\alpha} (\sigma_{i,k}^{\alpha})^2 + 2h^2 \tau^2 \sum_i \sum_k (\sum_{\alpha} \sigma_{i,k}^{\alpha})^2 + 2h\tau_0 \sum_i \sum_k \xi_{i,k} \sum_{\alpha} \sigma_{i,k}^{\alpha} \right]. \end{aligned} \quad (\text{A4})$$

Next, we consider the identity

$$e^{a^2} = \int_{-\infty}^{\infty} \frac{dx}{\sqrt{2\pi}} \exp \left[ -\frac{1}{2} x^2 + \sqrt{2}ax \right]. \quad (\text{A5})$$

A two-body problem is transformed into a one-body problem by this identity. This is called the Hubbard-Stratonovich transformation. Using the Hubbard-Stratonovich transformation, we rewrite the second term in the ferromagnetic term and the quadratic terms which appear in the prior probability distribution  $P(\{\xi\})$  (Eq. (15)) as follows.

$$\begin{aligned} \exp \left[ \frac{\beta_s}{N} (\sum_i \xi_i)^2 \right] &= \int_{-\infty}^{\infty} \frac{dm_0}{\sqrt{2\pi}} \exp \left[ -\frac{1}{2} m_0^2 + \sqrt{2}m_0 \sqrt{\frac{\beta_s}{N}} \sum_i \xi_i \right] \\ &= \sqrt{\frac{\beta_s N}{\pi}} \int_{-\infty}^{\infty} dm_0 \exp \left[ -N\beta_s m_0^2 + 2\beta_s m_0 \sum_i \xi_i \right] \end{aligned} \quad (\text{A6})$$

$$\begin{aligned}
\exp \left[ \frac{\beta_m}{N} \left( \sum_i \sigma_i^\alpha \right)^2 \right] &= \int_{-\infty}^{\infty} \frac{dm_\alpha}{\sqrt{2\pi}} \exp \left[ -\frac{1}{2} m_\alpha^2 + \sqrt{2} m_\alpha \sqrt{\frac{\beta_m}{N}} \sum_i \sigma_i^\alpha \right] \\
&= \sqrt{\frac{\beta_m N}{\pi}} \int_{-\infty}^{\infty} dm_\alpha \exp \left[ -N\beta_m m_\alpha^2 + 2\beta_m m_\alpha \sum_i \sigma_i^\alpha \right]
\end{aligned} \tag{A7}$$

where we changed the integral variables  $m_0$  and  $m_\alpha$  into  $\sqrt{2\beta_s N}m_0$  and  $\sqrt{2\beta_m N}m_\alpha$ . Averaging over the probability distribution  $P(\{\tau\}|\{\xi\})$  and using the above transformation, we obtain the averaged partition function  $[Z^n]$

$$\begin{aligned}
[Z^n] &= \text{tr}_\xi \int \prod_{i,k} d\tau_i^{(k)} \frac{1}{(\sqrt{2\pi}\tau)^{(Q-1)N}} \exp \left[ -\frac{1}{2\tau^2} \sum_i (\tau_i - \xi_i)^2 \right] \times \exp \left[ -\frac{\beta_s}{2N} \sum_{ij} (\xi_i - \xi_j)^2 \right] \\
&\quad \times \text{tr}_\sigma \exp \left[ -h \sum_i \sum_k \sum_\alpha (\tau_{i,k} - \sigma_{i,k}^\alpha)^2 - \frac{\beta_m}{2N} \sum_{ij} \sum_\alpha (\sigma_i^\alpha - \sigma_j^\alpha)^2 \right] \\
&= \frac{1}{Z(\beta_s)} \left( \frac{\beta_s N}{\pi} \right)^{\frac{1}{2}} \left( \frac{\beta_m N}{\pi} \right)^{\frac{n}{2}} \int_{-\infty}^{\infty} dm_0 \int_{-\infty}^{\infty} \prod_\alpha dm_\alpha e^{-N\beta_s m_0^2 - N\beta_m \sum_\alpha m_\alpha^2} \text{tr}_{\xi,\sigma} e^{L_1}
\end{aligned} \tag{A8}$$

where

$$\begin{aligned}
L_1 &= 2\beta_s m_0 \sum_i \xi_i + 2\beta_m \sum_\alpha m_\alpha \sum_i \sigma_i^\alpha - \beta_s \sum_i \xi_i^2 - \beta_m \sum_i \sum_\alpha (\sigma_i^\alpha)^2 \\
&\quad - h \sum_i \sum_\alpha \sum_k (\sigma_{i,k}^\alpha)^2 + 2h^2 \tau^2 \sum_i \sum_k (\sum_\alpha \sigma_{i,k}^\alpha)^2 + 2h\tau_0 \sum_i \sum_k \xi_{i,k} \sum_\alpha \sigma_{i,k}^\alpha.
\end{aligned} \tag{A9}$$

Since the summation over spin  $\sigma_i^\alpha$  in equation (A8) can be calculated at each site separately, we rewrite  $\text{Tr}_{\xi,\sigma} e^{L_1}$  in equation (A8) using  $\text{tr}$  for the sum of spin site,

$$\begin{aligned}
\text{tr}_{\xi,\sigma} e^{L_1} &= \left[ \text{tr}_{\xi,\sigma} e^{L_2} \right]^N \\
&= \exp \left[ N \ln \text{tr}_{\xi,\sigma} e^{L_2} \right]
\end{aligned} \tag{A10}$$

where

$$\begin{aligned}
L_2 &= 2\beta_s m_0 \xi + 2\beta_m \sum_\alpha m_\alpha \sigma^\alpha - \beta_s \xi^2 - \beta_m \sum_\alpha (\sigma^\alpha)^2 \\
&\quad - h \sum_\alpha \sum_k (\sigma_k^\alpha)^2 + 2h^2 \tau^2 \sum_k (\sum_\alpha \sigma_k^\alpha)^2 + 2h\tau_0 \sum_k \xi_k \sum_\alpha \sigma_k^\alpha.
\end{aligned} \tag{A11}$$

Furthermore, using the Hubbard-Stratonovich transformation to  $(\sum_\alpha \sigma_k^\alpha)^2$  in equation (A11) again

$$\begin{aligned}
\exp \left[ \left( \sqrt{2}h\tau \sum_\alpha \sigma_k^\alpha \right)^2 \right] &= \int_{-\infty}^{\infty} \frac{du_k}{\sqrt{2\pi}} \exp \left[ -\frac{1}{2} u_k^2 + 2h\tau u_k \sum_\alpha \sigma_k^\alpha \right] \\
&\equiv \int_{-\infty}^{\infty} Du_k \exp \left[ 2h\tau u_k \sum_\alpha \sigma_k^\alpha \right],
\end{aligned} \tag{A12}$$

the averaged partition function  $[Z^n]$  (A8) is rewritten as

$$\begin{aligned}
[Z^n] &\approx \int_{-\infty}^{\infty} dm_0 \int_{-\infty}^{\infty} \prod_\alpha dm_\alpha \exp \left[ -N\beta_s m_0^2 - N\beta_m \sum_\alpha m_\alpha^2 \right. \\
&\quad \left. + N \ln \text{tr}_{\xi,\sigma} \int Du_1 \cdots \int Du_{Q-1} e^{L_3} \right]
\end{aligned} \tag{A13}$$

where

$$\begin{aligned} L_3 = & 2\beta_s m_0 \xi + 2\beta_m \sum_{\alpha} m_{\alpha} \sigma^{\alpha} - \beta_s \xi^2 - \beta_m \sum_{\alpha} (\sigma^{\alpha})^2 \\ & - h \sum_{\alpha} \sum_k (\sigma_k^{\alpha})^2 + 2h\tau \sum_k u_k \sum_{\alpha} \sigma_k^{\alpha} + 2h\tau_0 \sum_k \xi_k \sum_{\alpha} \sigma_k^{\alpha}. \end{aligned} \quad (\text{A14})$$

The notation  $Du$  in equations (A12) and (A13) is called the Gaussian measure.

Here, we assume the replica symmetric ansatz:  $m_{\alpha} = m$  ( $\forall \alpha$ ). Since the replica is introduced to calculate the configurational average of free energy artificially, we may suppose that the averaged free energy does not depend upon the replica index. The solution under this assumption is called the replica-symmetric solution. Assuming replica symmetric ansatz, we can calculate a summation over spin  $\sigma^{\alpha}$  with respect to replica separately because the summation is similar to equation (A10). Then, since the argument of exponential function is proportional to  $N$ , the integral with respect to variables  $m_0$  and  $m$  can be evaluated by the saddle point method in the thermodynamic limit  $N \rightarrow \infty$ , and the averaged partition function (A13) becomes

$$\begin{aligned} [Z^n] \approx & \int_{-\infty}^{\infty} dm_0 \int_{-\infty}^{\infty} \prod_{\alpha} dm_{\alpha} \exp N \left[ -\beta_s m_0^2 - n\beta_m m^2 \right. \\ & \left. + \ln \text{tr}_{\xi} e^{2\beta_s m_0 \xi - \beta_s \xi^2} \int Du_1 \cdots \int Du_{Q-1} e^{n \ln \text{tr}_{\sigma} e^{\tilde{L}}} \right] \\ \approx & \exp N \left[ -\beta_s m_0^2 - n\beta_m m^2 + \ln \text{tr}_{\xi} e^{2\beta_s m_0 \xi - \beta_s \xi^2} \int Du_1 \cdots \int Du_{Q-1} e^{n \ln \text{tr}_{\sigma} e^{\tilde{L}}} \right] \\ \approx & 1 + nN \left[ -\frac{1}{n} \beta_s m_0^2 - \beta_m m + \frac{1}{n} \ln \text{tr}_{\xi} e^{2\beta_s m_0 \xi - \beta_s \xi^2} \int Du_1 \cdots \int Du_{Q-1} e^{n \ln \text{tr}_{\sigma} e^{\tilde{L}}} \right] \\ \approx & 1 + nN \left[ -\frac{1}{n} \beta_s m_0^2 - \beta_m m + \frac{1}{n} \ln \text{tr}_{\xi} e^{2\beta_s m_0 \xi - \beta_s \xi^2} \right. \\ & \left. + \frac{\text{tr}_{\xi} \int Du_1 \cdots \int Du_{Q-1} e^{2\beta_s m_0 \xi - \beta_s \xi^2} \ln \text{tr}_{\sigma} e^{\tilde{L}}}{\text{tr}_{\xi} e^{2\beta_s m_0 \xi - \beta_s \xi^2}} \right], \end{aligned} \quad (\text{A15})$$

where

$$\tilde{L} = 2\beta_m m \sigma - \beta_m \sigma^2 - h \sum_k \sigma_k^2 + 2h\tau \sum_k u_k \sigma_k + 2h\tau_0 \sum_k \xi_k \sigma_k. \quad (\text{A16})$$

During the calculation, we kept  $N$  large enough and brought  $n$  close to 0. The  $m_0$  and  $m$  take the extremum of function  $[\dots]$  in equation (A15). Then the free energy is given by equations (20) and (21). When we define the free energy as  $f(m_0, m) \equiv f_1(m_0) + n f_2(m)$ , where  $f_1$  is the  $n$ -independent term and  $f_2$  is the  $n$ -dependent term, each free energy is represented as,

$$f_1 = -\beta_s m_0^2 + \ln \text{tr}_{\xi} e^{2\beta_s m_0 \xi - \beta_s \xi^2}, \quad (\text{A17})$$

$$f_2 = -\beta_m m^2 + \frac{\text{tr}_{\xi} \int Du_1 \cdots \int Du_{Q-1} e^{2\beta_s m_0 \xi - \beta_s \xi^2} \ln \text{tr}_{\sigma} e^{\tilde{L}}}{\text{tr}_{\xi} e^{2\beta_s m_0 \xi - \beta_s \xi^2}}. \quad (\text{A18})$$

We next derive the saddle point equations for respect to  $m_0$  and  $m$ . The saddle point equations with respect to  $m_0$  and  $m$  are obtained by the conditions of extreme value,  $\partial f_1 / \partial m_0 = 0$ , and  $\partial f_2 / \partial m = 0$  and they are expressed as equations (23) and (24), respectively.

## APPENDIX B: DYNAMICAL PROPERTIES OF THE INFINITE-RANGE MODEL

In this appendix, we derive the differential equation (36) with respect to the macroscopic quantity  $m$  to analyze dynamical properties of image restoration in the infinite-range model. The macroscopic order parameter  $m$  is derived from the master equation (32).

We introduce the probability distribution of macroscopic magnetization  $\mathcal{P}_t(m)$ . Then the derivative of this probability distribution (35) with respect to  $t$  becomes

$$\begin{aligned}
\frac{d}{dt}\mathcal{P}_t(m) &= \sum_{\sigma} \frac{dp_t(\sigma)}{dt} \delta[m - m(\sigma)] \\
&= \sum_{\sigma} \sum_{k=1}^N \sum_{\sigma_{k'}=0}^{Q-1} \left[ \omega(\sigma_{k'} \rightarrow \sigma_k) p_t(\sigma') - \omega(\sigma_k \rightarrow \sigma_{k'}) p_t(\sigma) \right] \delta[m - m(\sigma)] \\
&= \sum_{\sigma} \sum_{k=1}^N \sum_{\sigma_{k'}=0}^{Q-1} \omega(\sigma_k \rightarrow \sigma_{k'}) p_t(\sigma) \left\{ \delta[m - m(\sigma)] + \frac{1}{N} (\sigma_k - \sigma_{k'}) \right. \\
&\quad \left. - \delta[m - m(\sigma)] \right\} \\
&= \frac{\partial}{\partial m} \left\{ \sum_{\sigma} \sum_{k=1}^N \sum_{\sigma_{k'}=0}^{Q-1} \omega(\sigma_k \rightarrow \sigma_{k'}) p_t(\sigma) \delta[m - m(\sigma)] \frac{1}{N} (\sigma_k - \sigma_{k'}) \right\}.
\end{aligned} \tag{B1}$$

Substituting Eq. (33) for the transition probability  $\omega(\sigma_k \rightarrow \sigma_{k'})$  to the above equation, we obtain

$$\begin{aligned}
\frac{d}{dt}\mathcal{P}_t(m) &= \frac{\partial}{\partial m} \left\{ \sum_{\sigma} \sum_{k=1}^N \sum_{\sigma_{k'}=0}^{Q-1} p_t(\sigma) \delta[m - m(\sigma)] \frac{1}{N} (\sigma_k - \sigma_{k'}) \right. \\
&\quad \times \frac{\exp[h_{\text{eff}}]}{\text{tr}_{\sigma_{k'}^{(1)}, \dots, \sigma_{k'}^{(Q-1)}} \exp[h_{\text{eff}}]} \left. \right\} \\
&= \frac{\partial}{\partial m} \left\{ \sum_{\sigma} p_t(\sigma) \delta[m - m(\sigma)] \right. \\
&\quad \times \left[ \frac{1}{N} \sum_{k=1}^N \sigma_k - \frac{1}{N} \sum_{k=1}^N \frac{\text{tr}_{\sigma_{k'}^{(1)}, \dots, \sigma_{k'}^{(Q-1)}} \exp[h_{\text{eff}}]}{\text{tr}_{\sigma_{k'}^{(1)}, \dots, \sigma_{k'}^{(Q-1)}} \exp[h_{\text{eff}}]} \right] \left. \right\}.
\end{aligned} \tag{B2}$$

Furthermore, substituting Eq. (35) to the above equation again and using  $m = (1/N) \sum_{k=1}^{Q-1} \sigma_k$ , we find that the above equation in the thermodynamic limit  $N \rightarrow \infty$  becomes

$$\begin{aligned}
\frac{d}{dt}\mathcal{P}_t(m) &= \frac{\partial}{\partial m} \left\{ m \mathcal{P}_t(m) \right\} \\
&\quad - \frac{\partial}{\partial m} \left\{ \mathcal{P}_t(m) \frac{\text{tr}_{\xi} e^{2m_0 \beta_s \xi - \beta_s \xi^2}}{Z(\beta_m)} \int Du_1 \cdots \int Du_{Q-1} \frac{\text{tr}_{\sigma} \sigma \exp(H_{\text{eff}})}{\text{tr}_{\sigma} \exp(H_{\text{eff}})} \right\} \\
&= \frac{\partial}{\partial m} \left\{ \mathcal{P}_t(m) \left[ m - \frac{\text{tr}_{\xi} e^{2m_0 \beta_s \xi - \beta_s \xi^2}}{Z(\beta_m)} \right. \right. \\
&\quad \left. \left. \times \int Du_1 \cdots \int Du_{Q-1} \frac{\text{tr}_{\sigma} \sigma \exp(H_{\text{eff}})}{\text{tr}_{\sigma} \exp(H_{\text{eff}})} \right] \right\}.
\end{aligned} \tag{B3}$$

Here we redefine the probability distribution  $\mathcal{P}_t(m)$  that the macroscopic magnetization is  $m$  at time  $t$  as

$$\mathcal{P}_t(m) = \delta[m - m(t)]. \tag{B4}$$

Multiplying  $m$  and integrating with  $m$  in both sides, we obtain the left hand side of equation (B3) as,

$$\begin{aligned}
\text{Left hand side} &= \int_{-\infty}^{\infty} m dm \frac{d}{dt} \mathcal{P}_t(m) = \int_{-\infty}^{\infty} m dm \frac{d}{dt} \delta[m - m(t)] \\
&= \frac{d}{dt} \int_{-\infty}^{\infty} m \delta[m - m(t)] dm = \frac{d}{dt} m(t).
\end{aligned} \tag{B5}$$

On the other hand, the right hand side is calculated as follows.

$$\begin{aligned}
\text{Right hand side} &= \int_{-\infty}^{\infty} m dm \frac{\partial}{\partial m} \left\{ \delta[m - m(t)] \left[ m - \frac{\text{tr}_{\xi} e^{2m_0 \beta_s \xi - \beta_s \xi^2}}{Z(\beta_m)} \right. \right. \\
&\quad \times \int Du_1 \cdots \int Du_{Q-1} \frac{\text{tr}_{\sigma} \sigma \exp(H_{\text{eff}})}{\text{tr}_{\sigma} \exp(H_{\text{eff}})} \left. \right] \left. \right\} \\
&= -m(t) + \frac{\text{tr}_{\xi} e^{2m_0 \beta_s \xi - \beta_s \xi^2}}{Z(\beta_m)} \int Du_1 \cdots \int Du_{Q-1} \frac{\text{tr}_{\sigma} \sigma \exp(H_{\text{eff}})}{\text{tr}_{\sigma} \exp(H_{\text{eff}})}. \tag{B6}
\end{aligned}$$

Thus we obtained the expression (36) as the time-dependent equation of magnetization. This expression can be written as

$$\frac{dm}{dt} \propto -\frac{\partial f_{\text{RS}}}{\partial m}$$

with the replica symmetric free energy  $f_{\text{RS}}$  and is referred to as the time-dependent Ginzburg-Landau equation. In the case of  $dm/dt = 0$ , this equation, obviously, corresponds to the saddle point equation (24) with respect to  $m$ .

### APPENDIX C: ASYMPTOTIC EXPRESSION OF $m$ AND $H_{\text{D}}$

The time-dependent magnetization we obtained in the previous appendix B should reduce to the magnetization of equilibrium state in the limit  $t \rightarrow \infty$ . Accordingly, we assume the asymptotic expression of magnetization  $m$  as equation (37). In this appendix, we derive the expression of relaxation time  $t_0$  and the asymptotic expression of the mean square error  $H_{\text{D}}$  corresponding to that of  $m$ .

We first substitute the expression (37) for the time-dependent Ginzburg-Landau equation (36) and consider the second term of the right hand side of Eq. (36).

$$\begin{aligned}
\text{tr}_{\sigma} e^{H_{\text{eff}}} &= \text{tr}_{\sigma} \exp[H'_{\text{eff}} + 2\beta_m \sigma m] \\
&= \text{tr}_{\sigma} \exp[H'_{\text{eff}} + 2\beta_m \sigma (\tilde{m} + a e^{-\frac{t}{t_0}})] \\
&= \text{tr}_{\sigma} \exp[\tilde{H}_{\text{eff}} + 2\beta_m \sigma a e^{-\frac{t}{t_0}}] \tag{C1}
\end{aligned}$$

where  $\tilde{H}_{\text{eff}}$  is the effective Hamiltonian of the static case (25). Using  $e^{-t/t_0} \rightarrow 0$  in the limit  $t \rightarrow \infty$ , we expand the right hand side of the above equation to first order.

$$\begin{aligned}
\text{tr}_{\sigma} e^{H_{\text{eff}}} &= \text{tr}_{\sigma} e^{\tilde{H}_{\text{eff}}} [1 + 2\beta_m \sigma a e^{-\frac{t}{t_0}} + (2\beta_m \sigma a)^2 e^{-\frac{2t}{t_0}} + \cdots] \\
&\approx \text{tr}_{\sigma} e^{\tilde{H}_{\text{eff}}} [1 + 2\beta_m \sigma a e^{-\frac{t}{t_0}}]. \tag{C2}
\end{aligned}$$

Then the thermal mean value appearing in the second term of the right hand side of equation (36) can be represented as

$$\begin{aligned}
\frac{\text{tr}_{\sigma} \sigma e^{H_{\text{eff}}}}{\text{tr}_{\sigma} e^{H_{\text{eff}}}} &\approx \frac{1}{2\beta_m} \frac{\partial}{\partial m} \log \text{tr}_{\sigma} e^{\tilde{H}_{\text{eff}}} [1 + 2\beta_m \sigma a e^{-\frac{t}{t_0}}] \\
&= \frac{1}{2\beta_m} \frac{\partial}{\partial m} \left\{ \log \left[ \text{tr}_{\sigma} e^{\tilde{H}_{\text{eff}}} \right] + \log \left[ 1 + 2\beta_m a e^{-\frac{t}{t_0}} \frac{\text{tr}_{\sigma} \sigma e^{\tilde{H}_{\text{eff}}}}{\text{tr}_{\sigma} e^{\tilde{H}_{\text{eff}}}} \right] \right\} \\
&\approx \frac{1}{2\beta_m} \frac{\partial}{\partial m} \left\{ \log \left[ \text{tr}_{\sigma} e^{\tilde{H}_{\text{eff}}} \right] + 2\beta_m a e^{-\frac{t}{t_0}} \frac{\text{tr}_{\sigma} \sigma e^{\tilde{H}_{\text{eff}}}}{\text{tr}_{\sigma} e^{\tilde{H}_{\text{eff}}}} \right\} \\
&= \frac{\text{tr}_{\sigma} \sigma e^{\tilde{H}_{\text{eff}}}}{\text{tr}_{\sigma} e^{\tilde{H}_{\text{eff}}}} + 2\beta_m a e^{-\frac{t}{t_0}} \left\{ \frac{\text{tr}_{\sigma} \sigma^2 e^{\tilde{H}_{\text{eff}}}}{\text{tr}_{\sigma} e^{\tilde{H}_{\text{eff}}}} - \left[ \frac{\text{tr}_{\sigma} \sigma e^{\tilde{H}_{\text{eff}}}}{\text{tr}_{\sigma} e^{\tilde{H}_{\text{eff}}}} \right]^2 \right\} \\
&\equiv \langle \sigma \rangle_{\tilde{H}_{\text{eff}}} + 2\beta_m a e^{-\frac{t}{t_0}} \left\{ \langle \sigma^2 \rangle_{\tilde{H}_{\text{eff}}} - \langle \sigma \rangle_{\tilde{H}_{\text{eff}}}^2 \right\}. \tag{C3}
\end{aligned}$$

We also approximated the thermal mean value to first order. Accordingly, the time-dependent Ginzburg-Landau equation (36) becomes

$$-\frac{a}{t_0}e^{-\frac{t}{t_0}} = -\tilde{m} - ae^{-\frac{t}{t_0}} + \frac{\text{tr}_\xi e^{2m_0\beta_s\xi - \beta_s\xi^2}}{Z(\beta_s)} \int Du_1 \cdots \int Du_{Q-1} \\ \times \left[ \langle \sigma \rangle_{\tilde{H}_{\text{eff}}} + 2\beta_m a e^{-\frac{t}{t_0}} \left\{ \langle \sigma^2 \rangle_{\tilde{H}_{\text{eff}}} - \langle \sigma \rangle_{\tilde{H}_{\text{eff}}}^2 \right\} \right],$$

and the inverse relaxation time  $t_0^{-1}$  is given by substituting the solution of the saddle point equation (24).

$$t_0^{-1} = 1 - \frac{2\beta_m}{Z_s} \text{tr}_\xi e^{2\beta_s m_0 \xi - \beta_s \xi^2} \int Du_1 \cdots \int Du_{Q-1} \left\{ \langle \sigma^2 \rangle_{\tilde{H}_{\text{eff}}} - \langle \sigma \rangle_{\tilde{H}_{\text{eff}}}^2 \right\}. \quad (\text{C4})$$

We next derive the asymptotic expression of the mean square error. The expectation value is divided into the time-dependent term and the time-independent term as we did in the previous calculation.

$$\langle \sigma \rangle = \frac{\text{tr}_\sigma \sigma e^{H_{\text{eff}}}}{\text{tr}_\sigma e^{H_{\text{eff}}}} = \langle \sigma \rangle_{\tilde{H}_{\text{eff}}} + 2\beta_m a e^{-\frac{t}{t_0}} \left\{ \langle \sigma^2 \rangle_{\tilde{H}_{\text{eff}}} - \langle \sigma \rangle_{\tilde{H}_{\text{eff}}}^2 \right\} \\ \equiv \langle \sigma \rangle_{\tilde{H}_{\text{eff}}} + R,$$

where we have rewritten the second term of the above expression  $R$  for simplification. Then the first order expansion of the step function  $\Theta(\langle \sigma \rangle)$  in the limit  $e^{-t/t_0} \rightarrow 0$  ( $t \rightarrow \infty$ ) is calculated as

$$\Theta \left( \langle \sigma \rangle - \frac{2k-1}{2} \right) = \Theta \left( \langle \sigma \rangle_{\tilde{H}_{\text{eff}}} + R - \frac{2k-1}{2} \right) \\ \approx \Theta \left( \langle \sigma \rangle_{\tilde{H}_{\text{eff}}} + R - \frac{2k-1}{2} \right) \Big|_{R=0} \\ + \frac{R}{1!} \left\{ \Theta' \left( \langle \sigma \rangle_{\tilde{H}_{\text{eff}}} + R - \frac{2k-1}{2} \right) \Big|_{R=0} \right\} \\ \approx \Theta \left( \langle \sigma \rangle_{\tilde{H}_{\text{eff}}} - \frac{2k-1}{2} \right) + R \delta \left( \langle \sigma \rangle_{\tilde{H}_{\text{eff}}} - \frac{2k-1}{2} \right). \quad (\text{C5})$$

The function  $\Omega$  consists of the step functions  $\Theta$  (see Eq. (9)). Accordingly, using the above first order expansion of the step function  $\Theta(\langle \sigma \rangle)$ , we obtain the expansion of  $\Omega(\langle \sigma \rangle)$  to first order is given as

$$\Omega(\langle \sigma \rangle) \approx \Omega(\langle \sigma \rangle_{\tilde{H}_{\text{eff}}}) + R \sum_{k=1}^Q k \left[ \delta \left( \langle \sigma \rangle_{\tilde{H}_{\text{eff}}} - \frac{2k-1}{2} \right) - \delta \left( \langle \sigma \rangle_{\tilde{H}_{\text{eff}}} - \frac{2k+1}{2} \right) \right] \\ \equiv \Omega(\langle \sigma \rangle_{\tilde{H}_{\text{eff}}}) + X, \quad (\text{C6})$$

where we have rewritten the second term of the above expression  $X$  for simplification, and the asymptotic expression of  $[\xi - \Omega(\langle \sigma \rangle)]^2$  becomes

$$\left[ \xi - \Omega(\langle \sigma \rangle) \right]^2 \approx \left[ \xi - \Omega(\langle \sigma \rangle) \Big|_{X=0} \right]^2 + 2 \left[ \xi - \Omega(\langle \sigma \rangle) \Big|_{X=0} \right] X. \quad (\text{C7})$$

Therefore we obtain the asymptotic expression of the mean square error in the limit  $t \rightarrow \infty$  as

$$H_D(m) = \frac{1}{Z(\beta_s)} \text{tr}_\xi e^{2m_0\beta_s\xi - \beta_s\xi^2} \int Du_1 \cdots \int Du_{Q-1} \\ \left\{ \left[ \xi - \Omega(\langle \sigma \rangle_{\tilde{H}_{\text{eff}}}) \right]^2 + 2 \left[ \xi - \Omega(\langle \sigma \rangle_{\tilde{H}_{\text{eff}}}) \right] X \right\} \\ = H_D(\tilde{m})$$

$$\begin{aligned}
& + 4\beta_m a e^{-\frac{t}{t_0}} \frac{1}{Z(\beta_s)} \text{tr}_\xi e^{2m_0 \beta_s \xi - \beta_s \xi^2} \int Du_1 \cdots \int Du_{Q-1} \left[ \xi - \Omega(\langle \sigma \rangle_{\tilde{H}_{\text{eff}}}) \right] \\
& \times \sum_{k=1}^Q k \left[ \delta \left( \langle \sigma \rangle_{\tilde{H}_{\text{eff}}} - \frac{2k-1}{2} \right) - \delta \left( \langle \sigma \rangle_{\tilde{H}_{\text{eff}}} - \frac{2k+1}{2} \right) \right] \left[ \langle \sigma^2 \rangle_{\tilde{H}_{\text{eff}}} - \langle \sigma \rangle_{\tilde{H}_{\text{eff}}}^2 \right] \\
& = H_D(\tilde{m}) + b e^{-\frac{t}{t_0}}. \tag{C8}
\end{aligned}$$

#### APPENDIX D: MEAN-FIELD ANNEALING

We calculate the restored image for realistic pictures in two dimensions by the mean-field annealing. In order to use the mean-field annealing, we need the recursion relation for the iterative algorithm as equation (45). The recursion relation with respect to magnetization  $m$  is given from a mean-field approximation here. In this appendix, we derive the recursion relation (45) from partial differentiation of the free energy. Instead of expression (44), we consider the following,

$$\mathcal{L} = \mathcal{E}(\rho) + T_m \mathcal{S}(\rho) + \sum_{(ij)}^N \lambda_{ij} \left( \sum_{\sigma_{ij}=0}^{Q-1} \rho_{ij}(\sigma_{ij}) - 1 \right), \tag{D1}$$

where  $\lambda_{ij}$  is the Lagrange multiplier. We introduced the constraint condition,  $\sum_{\sigma_{ij}=0}^{Q-1} \rho_{ij}(\sigma_{ij}) = 1$ , by using the Lagrange multiplier. The expressions of the energy  $\mathcal{E}$  and entropy  $\mathcal{S}$  approximated by equation (43) are given respectively as,

$$\begin{aligned}
\mathcal{E}(\rho) & \approx \sum_{\sigma_{1,1}=0}^{Q-1} \cdots \sum_{\sigma_{Lx,Ly}=0}^{Q-1} H_{\text{eff}} \prod_{(ij)} \rho_{ij}(\sigma_{ij}) \\
& = \sum_{\sigma_{1,1}=0}^{Q-1} \cdots \sum_{\sigma_{i,j}=0}^{Q-1} \cdots \sum_{\sigma_{k,l}=0}^{Q-1} \cdots \sum_{\sigma_{Lx,Ly}=0}^{Q-1} H_{\text{eff}} \\
& \quad \times \rho_{11}(\sigma_{11}) \cdots \rho_{ij}(\sigma_{ij}) \cdots \rho_{kl}(\sigma_{kl}) \cdots \rho_{LxLy}(\sigma_{LxLy}), \tag{D2}
\end{aligned}$$

$$\begin{aligned}
\mathcal{S}(\rho) & \approx - \sum_{\sigma_{1,1}=0}^{Q-1} \cdots \sum_{\sigma_{Lx,Ly}=0}^{Q-1} \prod_{(ij)} \rho_{ij}(\sigma_{ij}) \ln \prod_{(ij)} \rho_{ij}(\sigma_{ij}) \\
& = \sum_{\sigma_{1,1}=0}^{Q-1} \cdots \sum_{\sigma_{i,j}=0}^{Q-1} \cdots \sum_{\sigma_{k,l}=0}^{Q-1} \cdots \sum_{\sigma_{Lx,Ly}=0}^{Q-1} \rho_{11}(\sigma_{11}) \cdots \rho_{ij}(\sigma_{ij}) \cdots \rho_{kl}(\sigma_{kl}) \cdots \\
& \quad \times \rho_{LxLy}(\sigma_{LxLy}) \sum_{ij} \ln \rho_{ij}(\sigma_{ij}) \tag{D3}
\end{aligned}$$

where the notation  $ij$  represents the site index on a two-dimensional lattice with size  $L_x \times L_y$ . Then the variation of Lagrangian with respect to  $\rho_{ij}$  is

$$\begin{aligned}
\frac{\partial \mathcal{L}}{\partial \rho_{ij}} & = \sum_{\sigma_{ij}} \left[ \sum_{\sigma_{1,1}=0}^{Q-1} \cdots \sum_{\sigma_{k,l}=0}^{Q-1} \cdots \sum_{\sigma_{Lx,Ly}=0}^{Q-1} \rho_{11}(\sigma_{11}) \cdots \rho_{kl}(\sigma_{kl}) \cdots \rho_{LxLy}(\sigma_{LxLy}) H_{\text{eff}} \right. \\
& \quad \left. + T_m \sum_{\sigma_{1,1}=0}^{Q-1} \cdots \sum_{\sigma_{k,l}=0}^{Q-1} \cdots \sum_{\sigma_{Lx,Ly}=0}^{Q-1} \rho_{11}(\sigma_{11}) \cdots \rho_{kl}(\sigma_{kl}) \cdots \rho_{LxLy}(\sigma_{LxLy}) \right. \\
& \quad \left. \times \sum_{ij \neq kl} \ln \rho_{kl}(\sigma_{kl}) + T_m \ln \rho_{ij}(\sigma_{ij}) + T_m + \lambda_{ij} \right] \\
& = 0 \tag{D4}
\end{aligned}$$

This leads to

$$\begin{aligned} \ln \rho_{ij}(\sigma_{ij}) &= -\frac{1}{T_m} \sum_{\sigma_{1,1}=0}^{Q-1} \cdots \sum_{\sigma_{k,l}=0}^{Q-1} \cdots \sum_{\sigma_{Lx,Ly}=0}^{Q-1} \rho_{11}(\sigma_{11}) \cdots \rho_{kl}(\sigma_{kl}) \cdots \rho_{LxLy}(\sigma_{LxLy}) H_{\text{eff}} \\ &\quad - a - \frac{\lambda_{ij}}{T_m}, \end{aligned} \quad (\text{D5})$$

where  $a$  is the constant without depending on a site  $(ij)$ . Consequently, the marginal probability distribution  $\rho_{ij}(\sigma_{ij})$  with respect to site  $ij$  becomes

$$\rho_{ij}(\sigma_{ij}) = e^{-\frac{\lambda_{ij}}{T_m} - a} e^{-\frac{1}{T_m} \sum_{\sigma_{1,1}=0}^{Q-1} \cdots \sum_{\sigma_{k,l}=0}^{Q-1} \cdots \sum_{\sigma_{Lx,Ly}=0}^{Q-1} \rho_{11}(\sigma_{11}) \cdots \rho_{kl}(\sigma_{kl}) \cdots \rho_{LxLy}(\sigma_{LxLy}) H_{\text{eff}}}. \quad (\text{D6})$$

Then, since we obtain the following normalization constant,

$$e^{-\frac{\lambda_{ij}}{T_m} - a} = \left[ \sum_{\sigma_{ij}} e^{-\frac{1}{T_m} \sum_{\sigma_{1,1}=0}^{Q-1} \cdots \sum_{\sigma_{k,l}=0}^{Q-1} \cdots \sum_{\sigma_{Lx,Ly}=0}^{Q-1} \rho_{11}(\sigma_{11}) \cdots \rho_{kl}(\sigma_{kl}) \cdots \rho_{LxLy}(\sigma_{LxLy}) H_{\text{eff}}} \right]^{-1},$$

by the constraint condition, the marginal probability distribution is expressed as

$$\rho_{ij}(\sigma_{ij}) = \frac{e^{-\frac{1}{T_m} \sum_{\sigma_{1,1}=0}^{Q-1} \cdots \sum_{\sigma_{k,l}=0}^{Q-1} \cdots \sum_{\sigma_{Lx,Ly}=0}^{Q-1} \rho_{11}(\sigma_{11}) \cdots \rho_{kl}(\sigma_{kl}) \cdots \rho_{LxLy}(\sigma_{LxLy}) H_{\text{eff}}}}{\sum_{\sigma_{ij}} e^{-\frac{1}{T_m} \sum_{\sigma_{1,1}=0}^{Q-1} \cdots \sum_{\sigma_{k,l}=0}^{Q-1} \cdots \sum_{\sigma_{Lx,Ly}=0}^{Q-1} \rho_{11}(\sigma_{11}) \cdots \rho_{kl}(\sigma_{kl}) \cdots \rho_{LxLy}(\sigma_{LxLy}) H_{\text{eff}}}}. \quad (\text{D7})$$

Next, we consider the argument of the exponential function in the above equation (D7). The effective Hamiltonian  $H_{\text{eff}}$  in two dimensions is given by

$$\begin{aligned} H_{\text{eff}} &= \frac{\beta_m}{2} \sum_{m,n} \left\{ (\sigma_{m,n} - \sigma_{m+1,n})^2 + (\sigma_{m,n} - \sigma_{m-1,n})^2 + (\sigma_{m,n} - \sigma_{m,n+1})^2 \right. \\ &\quad \left. + (\sigma_{m,n} - \sigma_{m,n-1})^2 \right\} + h \sum_{m,n} \sum_{p=1}^{Q-1} (\tau_{m,n,(p)} - \sigma_{m,n,(p)})^2 \\ &= -\beta_m \sum_{m,n} (\sigma_{m+1,n} + \sigma_{m-1,n} + \sigma_{m,n+1} + \sigma_{m,n-1}) \sigma_{m,n} \\ &\quad + \frac{\beta_m}{2} \sum_{m,n} (4\sigma_{m,n}^2 + \sigma_{m+1,n}^2 + \sigma_{m-1,n}^2 + \sigma_{m,n+1}^2 + \sigma_{m,n-1}^2) \\ &\quad + h \sum_{m,n} \sum_{p=1}^{Q-1} (\tau_{m,n,(p)} - \sigma_{m,n,(p)})^2 \end{aligned} \quad (\text{D8})$$

where  $m, n$  is the site index in two dimensions and  $p$  is the label of bit-decomposed data. When we take notice of a site  $(i, j)$  and distinguish the term related to site  $(i, j)$  and other terms, the above effective Hamiltonian becomes

$$\begin{aligned} H_{\text{eff}} &= -\beta_m (\sigma_{i+1,j} + \sigma_{i-1,j} + \sigma_{i,j+1} + \sigma_{i,j-1}) \sigma_{i,j} + 2\beta_m \sigma_{i,j}^2 + h \sum_{p=1}^{Q-1} \{\sigma_{i,j,(p)}\}^2 \\ &\quad - 2h \sum_{p=1}^{Q-1} \tau_{i,j,(p)} \sigma_{i,j,(p)} - \beta_m \sum_{kl \neq ij} (\sigma_{k+1,l} + \sigma_{k-1,l} + \sigma_{k,l+1} + \sigma_{k,l-1}) \sigma_{k,l} \\ &\quad + 2\beta_m \sum_{kl \neq ij} \sigma_{k,l}^2 + h \sum_{p=1}^{Q-1} \sum_{kl \neq ij} \{\sigma_{k,l,(p)}\}^2 - 2h \sum_{p=1}^{Q-1} \sum_{kl \neq ij} \tau_{k,l,(p)} \sigma_{k,l,(p)} \end{aligned}$$

$$+h \sum_{p=1}^{Q-1} \sum_{m,n} \{\tau_{m,n,(p)}\}^2. \quad (\text{D9})$$

Here, using the relation between the local magnetization and marginal distribution as

$$m_{i(\pm 1),j(\pm 1)} = \sum_{\sigma}^{Q-1} \sigma_{i(\pm 1),j(\pm 1)} \rho_{i(\pm 1),j(\pm 1)}(\sigma_{i(\pm 1),j(\pm 1)}),$$

we obtain the marginal probability distribution under the mean-field approximation,

$$\begin{aligned} \rho_{i,j}(\sigma_{i,j}) &= \frac{\exp[H_{\text{MF}}/T_m]}{\text{tr}_{\sigma} \exp[H_{\text{MF}}/T_m]} \\ &= \frac{1}{Z_{\text{MF}}} \exp[H_{\text{MF}}/T_m] \end{aligned} \quad (\text{D10})$$

where the Hamiltonian in the mean-field approximation  $H_{\text{MF}}$  is given in equation (46). In addition, the above local magnetization at site  $(i, j)$  can be represented as

$$m_{i,j} = \frac{1}{Z_{\text{MF}}} \text{tr}_{\sigma} \sigma_{i,j} e^{\frac{H_{\text{MF}}}{T_m}}, \quad (\text{D11})$$

and we update the pixel value from the time  $t$  to  $t + 1$  by using this relation (see (45)).

Original Image	$H_D^{\text{opt.}}$	NNP1–O	NNP1–D	NNP1–R
chair(BDD)	0.10467500	0.827925	0.023925	0.870800
chair(Q-Ising)	0.13967500	0.827925	0.127746	0.849700
girl(BDD)	0.22960000	0.552725	0.019000	0.636575
girl(Q-Ising)	0.26657500	0.552725	0.092100	0.452850
house(BDD)	0.38037500	0.538375	0.018000	0.374400
house(Q-Ising)	0.36840000	0.538375	0.079225	0.469675
lena(BDD)	0.35317500	0.450500	0.016575	0.467425
lena(Q-Ising)	0.34800000	0.450500	0.056086	0.449450
mant(BDD)	0.64400000	0.147900	0.008950	0.136975
mant(Q-Ising)	0.55120000	0.147900	0.021750	0.111100

TABLE I: Comparison of performance between our method and the  $Q$ -Ising form. The ratios of pixels at which the nearest neighboring pixels take the same value in the original image, the degraded image and restored image are represented as 'NNP1'.

Original Image	NNP2–O	NNP2–D	NNP2–R	$H_D^{\text{opt.}}$
chair(BDD)	0.955475	0.522025	0.998600	0.10467500
chair(Q-Ising)	0.955475	0.476000	0.999750	0.13967500
girl(BDD)	0.945025	0.450400	0.993850	0.22960000
girl(Q-Ising)	0.945025	0.438650	0.979750	0.26657500
house(BDD)	0.838400	0.442450	0.959600	0.38037500
house(Q-Ising)	0.838400	0.430775	0.967225	0.36840000
lena(BDD)	0.879325	0.413950	0.989825	0.35317500
lena(Q-Ising)	0.879325	0.402920	0.981625	0.34800000
mant(BDD)	0.615325	0.298100	0.934050	0.64400000
mant(Q-Ising)	0.615325	0.272400	0.801025	0.55120000

TABLE II: Ratio of pixel at which the difference among the value of the nearest neighboring pixels is smaller than 2 in the original, degraded and restored images.

Original Image	$H_D^{\text{opt.}}$	NNP–O	NNP–D	NNP–R
chair(BDD)	0.15512500	0.827925	0.006525	0.873225
chair(Q-Ising)	0.34862500	0.827925	0.050550	0.629175
girl(BDD)	0.34907500	0.552725	0.007175	0.653800
girl(Q-Ising)	0.51250000	0.552725	0.044300	0.519775
house(BDD)	0.53577500	0.538375	0.006625	0.485500
house(Q-Ising)	0.62777500	0.538375	0.034900	0.276275
lena(BDD)	0.54720000	0.450500	0.005400	0.507025
lena(Q-Ising)	0.48840000	0.450500	0.024625	0.543100
mant(BDD)	0.89227500	0.147900	0.004225	0.469375
mant(Q-Ising)	0.76495000	0.147900	0.008175	0.254500

TABLE III: Comparison of performance between using our method and the  $Q$ -Ising form for five standard images when  $H_D^{\tau} \sim 2.0$ . In this case, the restoration using our method is more efficient than that using the  $Q$ -Ising form in three standard images: "chair", "girl" and "house".

Original Image	Composition	BDD	$Q$ -Ising
chair	0.09427500	0.10467500	0.13967500
girl	0.18190000	0.22960000	0.26657500
house	0.32717500	0.38037500	0.36840000
lena	0.25742500	0.35317500	0.34800000
mant	0.52147500	0.64400000	0.55120000

TABLE IV: Comparison of performance among using our method, the  $Q$ -Ising form and the composition for five standard images when  $H_D^\tau \sim 1.0$ . In this case, the restoration using the composition is more efficient than that using our method and the  $Q$ -Ising form in all standard images.

## REFERENCES

- [1] H. Nishimori, *Statistical Physics of Spin Glass and Information Theory : An Introduction*, Oxford University Press (2001), in press.
- [2] Y. Kabashima and D. Saad, *Europhys. Lett.*, **44**, 668 (1998).
- [3] Y. Kabashima and D. Saad, *Europhys. Lett.*, **45**, 97 (1999).
- [4] Y. Kabashima, T. Murayama and D. Saad, *Phys. Rev. Lett.* **84**, 1355 (2000).
- [5] S. Geman and D. Geman, *Trans. on Pattern Anal. Mach. Intel.*, **PAMI-6**, 721 (1984).
- [6] D. Geiger and F. Girosi, *IEEE Trans. on Pattern. Anal. Mach. Intel.* **13**, 401 (1991).
- [7] J. M. Pryce and A. D. Bruce, *J. Phys. A: Math. Gen.* **28**, 511 (1995).
- [8] A. Cavagna, J. P. Gaorahan, I. Giardina and D. Sherrington, *Phys. Rev. Lett.* **83**, 4429 (1999).
- [9] D. Challet, M. Marsili and R. Zechina, *Phys. Rev. Lett.* **84**, 1824 (2000).
- [10] Y. Fu and P. W. Anderson, *J. Phys. A: Math. Gen.* **19**, 1605 (1986).
- [11] J. Inoue, *J. Phys. A: Math. Gen.* **30**, 1047 (1997).
- [12] F. F. Ferreira and J. F. Fontanari, *J. Phys. A: Math. Gen.* **31**, 3417 (1998).
- [13] D. Sherrington and S. Kirkpatrick, *Phys. Rev. Lett.* **35**, 1792 (1975).
- [14] T. Tanaka, "Analysis on bit error probability of direct-sequence CDMA multiuser demodulators", Proceedings of the conference Information-Based Induction Science : IBIS2000, pp. 57-63, (2000) (In Japanese).
- [15] J. Marroquin, S. Mitter, and T. Poggio, *J. Am. Stat. Assoc.* **82**, 76 (1987).
- [16] H. Nishimori and K. Y. M. Wong, *Phys. Rev. E* **60**, 132 (1999).
- [17] K. Tanaka, The Transaction on The Institute of Electronics, Information and Communication Engineers, **J82-A-10**, 1679 (1999) (In Japanese).
- [18] H. Nishimori, *Phys. Rev. B*, **27**, 5644 (1983).
- [19] H. Nishimori, *Phys. Rev. B*, **28**, 4011 (1983).
- [20] D. Bolle', H. Rieger and G. M. Shim, *J. Phys. A: Math. Gen.* **27**, 3411 (1994).
- [21] D. M. Carlucci and J. Inoue, *Phys. Rev. E* **60**, 2547 (1999).
- [22] J. Inoue and D. M. Carlucci, cond-mat/0006387.
- [23] Y. Iba, Proceeding of the Institute of Statistical Mathematics, **39**, 1 (1991) (In Japanese).
- [24] Y. Iba, BUSSEI KENKYUU, **60-6**, 677 (1993), supplement and revision, BUSSEI KENKYUU, **65-5**, 678 (1996) (In Japanese).
- [25] D. J. C. Mackay, *IEEE Transactions on Information Theory*, March (1999).
- [26] K. Tanaka and T. Morita, The Transaction on The Institute of Electronics, Information and Communication Engineers, **J80-A-6**, 1033 (1997) (In Japanese).
- [27] K. Tanaka, M. Ichioka and T. Morita, The Transaction on The Institute of Electronics, Information and Communication Engineers, **J80-A-1**, 260 (1997) (In Japanese).
- [28] The standard images which are used in this thesis are available at <ftp://ftp.lab1.kuis.kyoto-u.ac.jp/pub/sidba/>.
- [29] J. Inoue and K. Tanaka, "Dynamical properties of algorithms for image restoration by means of Bayesian statistics", Technical report of IEICE., **PRMU2000-124**, 33 (2000) (In Japanese).
- [30] Y. Iba, "Microcanonical and multicanonical approach to Bayesian image restoration", Research Memorandum No. 756, 08 June (2000).
- [31] T. Morita and K. Tanaka, *Physica A*, **223**, 244 (1996).

FIG. 1: The relation between the local magnetization  $\langle \sigma \rangle$  and the function  $\Omega$ .

FIG. 2: The example of decomposition by means of the method of threshold division in the  $Q = 3$  and 6-site case.

FIG. 3: The restoration process of gray-scale image. The upper process is the restoration of gray-scale image using the  $Q$ -Ising form. The lower process is the restoration of gray-scale image using the bit-decomposed data.

FIG. 4: Magnetization of the original image as a function of the source temperature for  $Q = 3$ . The solid line corresponds to a globally stable solution  $m_0 = 1$  and the dotted lines correspond to locally stable solutions  $m_0 = 0$  and  $m_0 = 1$ .

FIG. 5: The magnetization  $m$  and corresponding free energy  $f_{RS}$  are plotted in the upper-left and upper-right figures. The mean square error is plotted in the lower-left figure. The lower-right figure represents an enhancement of the mean square error around the optimal values. The solid line corresponds to the globally stable solution.

FIG. 6: Left figure is the mean square error as a function of temperature for several  $H$ . The solid line corresponds to the optimal value,  $T_m = T_s$ . Right figure represents comparison between the mean square error in the bit-decomposed data and the  $Q$ -Ising form for the optimal hyper-parameters  $H = H^{\text{opt}}$ . The solid line is that for the BDD case and the dotted line is the  $Q$ -Ising case.

FIG. 7: The time-dependence of magnetization  $m(t)$  is plotted in the upper left figure and the corresponding mean square error  $H_D(t)$  is plotted in the upper right figure for the optimal hyper-parameters  $T_m = 0.75$  and  $H = 0.75$ . Initial values of magnetization take from 0 to 3. The mean square error converges to its optimal value for any initial state of dynamics. The time-dependence of the magnetization  $m(t)$  (the lower left) and the mean square error  $H_D(t)$  for the hyper-parameters  $T_m = 0.3$  and  $H = 0.3$  (the lower right). Initial states of dynamics take from 0 to 2.5. The mean square error converges to the wrong state which is higher than the distance between the original and the degraded images, that is,  $H_D^{\tau} = 1.0$ .

FIG. 8: The inverse relaxation time  $t_0^{-1}$  as a function of temperature for several hyper-parameters  $H$  in the case of  $Q = 3$ ,  $T_s = 0.75$ ,  $\tau_0 = 1.0$  and  $\tau = 1/\sqrt{2}$ . The solid line is the inverse relaxation time at the optimal hyper-parameters  $H = H^{\text{opt}}$ .

FIG. 9: The magnetization of the  $Q$ -Ising model is simulated by Monte Carlo method. It is averaged over ten samples that are averages over 5000 MCS (15000 MCS – 10000 MCS). System size is  $100 \times 100$ . The left figure represents the magnetization as a function of temperature for  $Q = 4$  and the right figure is the magnetization as a function of temperature for  $Q = 8$ .

FIG. 10: The mean square error in the  $Q = 4$  case is calculated by Monte Carlo simulation (the upper figure). Averages over ten samples that (system size is  $100 \times 100$ ) is taken at each data point. The ratio of hyper-parameters  $H$  is chosen to be  $H = 0.6, 0.75$  (optimal) and  $1.0$ . The mean square error when  $Q = 8$ ,  $p = 0.15$ ,  $H_D^{\tau} \sim 1.0$  (the lower figures). The lower left figure represents the mean square error in  $T_s = 0.4$ , and the ratio of hyper-parameters  $H$  is chosen to be  $H = 0.6, 0.68$  (optimal) and  $0.8$ . The lower right figure represents the mean square error in  $T_m = 0.6$ , and the ratio of hyper-parameters  $H$  is chosen to be  $H = 0.8, 1.0$  (optimal) and  $1.2$ .

FIG. 11: Standard images: "chair", "girl", "house", "lena" and "mant".

FIG. 12: Standard image "lena". Left side figures represent the restoration using the bit-decomposed data, and right side figures represent the restoration using the  $Q$ -Ising form for  $H_D^{\tau} \sim 1.0$ .

FIG. 13: Standard image "lena". Left side figures represent the restoration using the bit-decomposed data, and right side figures represent the restoration using the  $Q$ -Ising form for  $H_D^{\tau} \sim 2.0$ .

FIG. 14: Restoration processes using the composition of both our method and the  $Q$ -Ising form. In the upper process (first process), we decompose a  $Q$ -value degraded image into  $Q - 1$  sets of binary degraded images after we received a  $Q$ -value degraded image. Using the binary degraded images, we restore the original image. On the other hand, in the lower process (second process), we received  $Q - 1$  sets of binary degraded images. After they are translated into a  $Q$ -value degraded image, we restore the original image using the  $Q$ -Ising form.

FIG. 15: Standard image “lena”. The left, center and right figures are the original, degraded and restored images, respectively, in the composition process when  $H_D^T \sim 1.0$ .

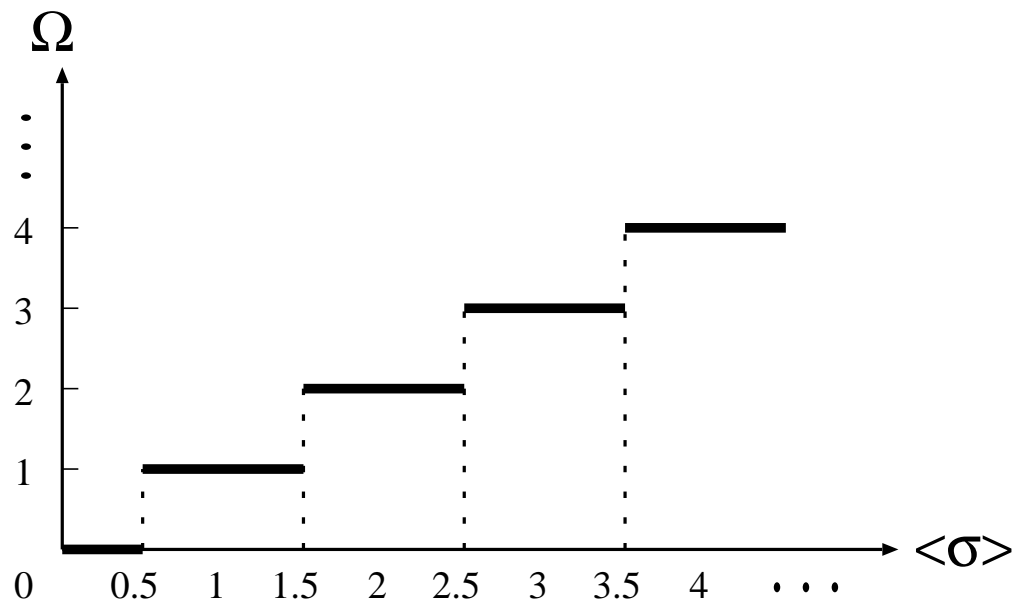


FIG. 1  
Tadaki and Inoue

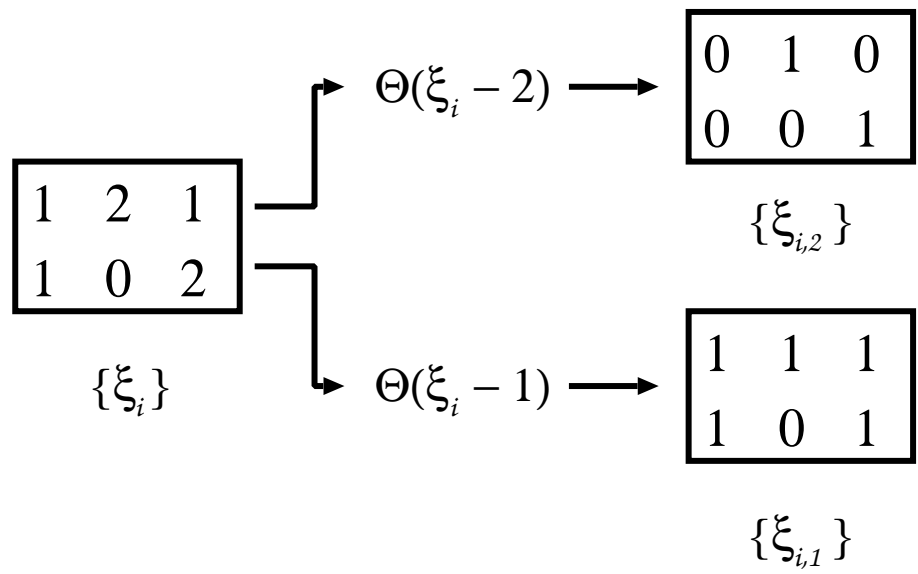


FIG. 2  
Tadaki and Inoue

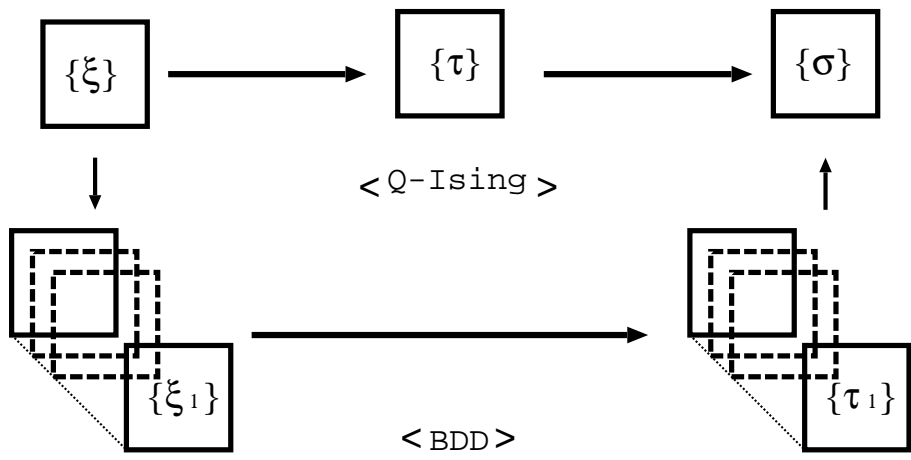


FIG. 3  
Tadaki and Inoue

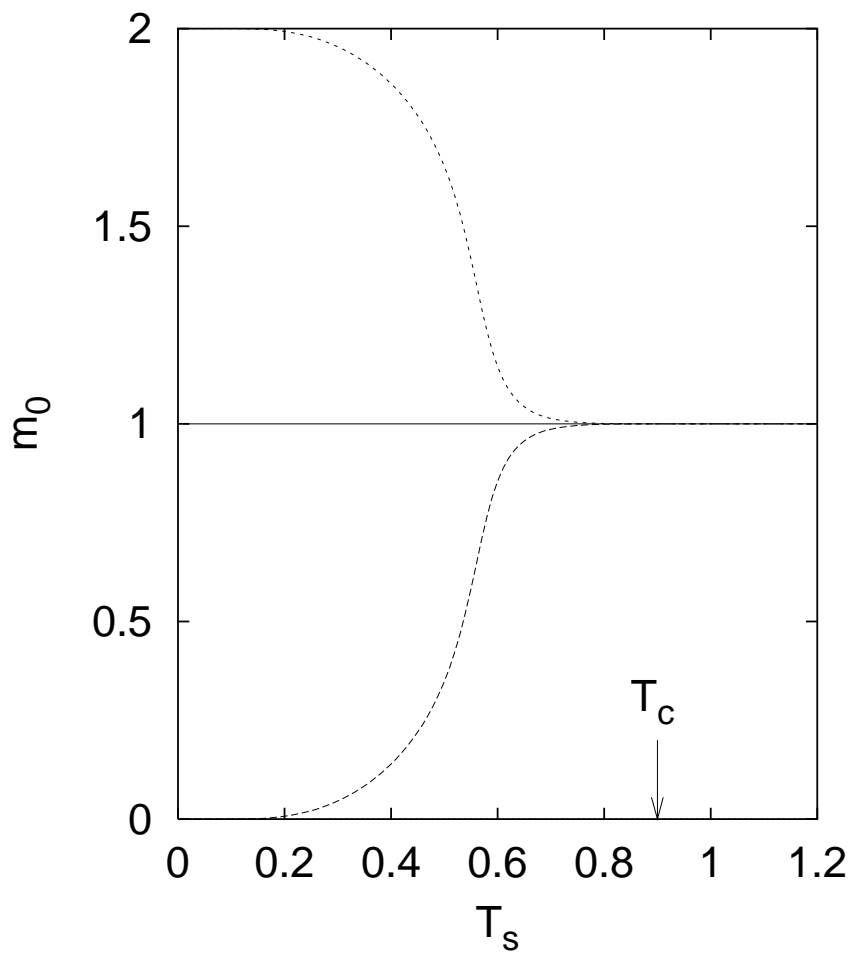
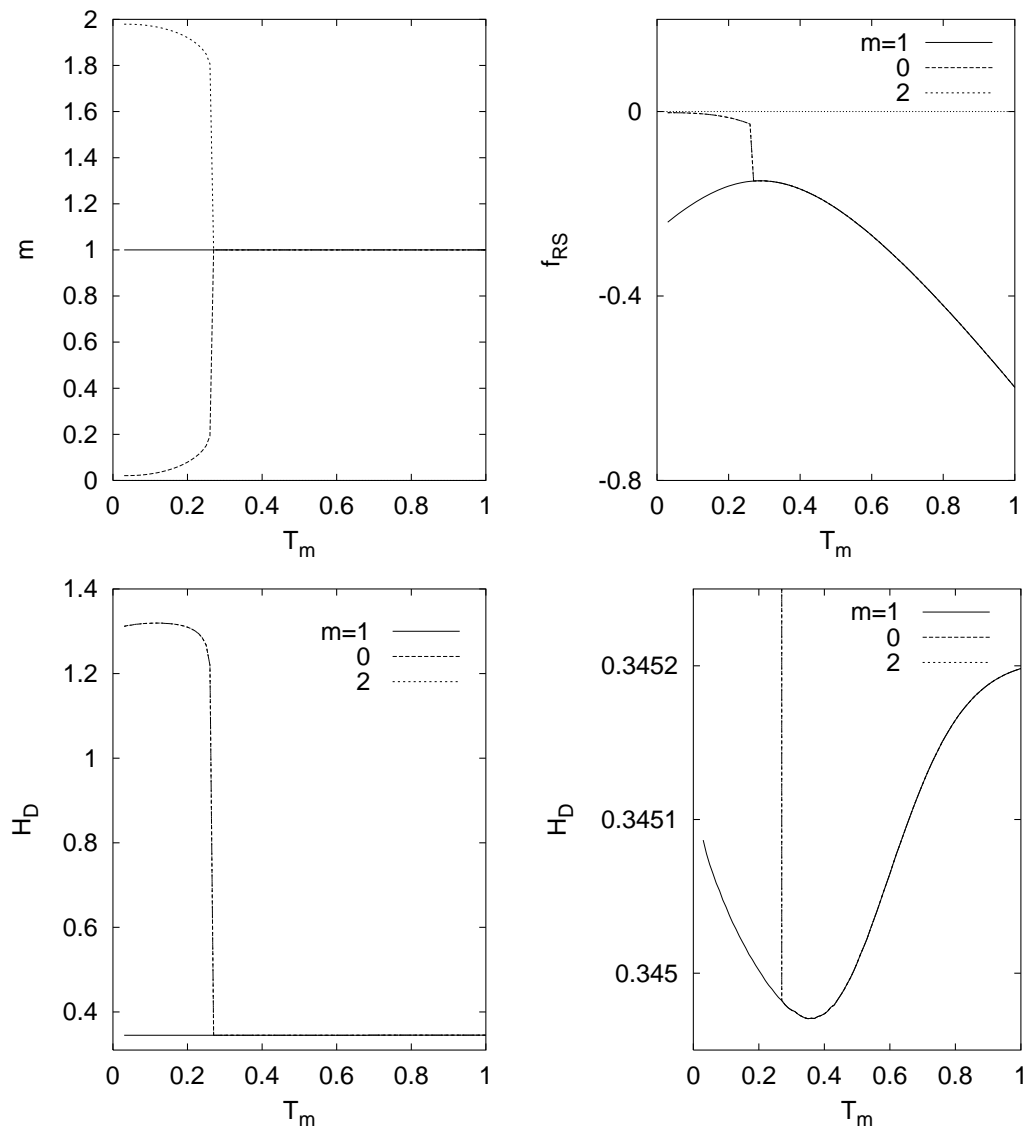


FIG. 4  
Tadaki and Inoue



**FIG. 5**  
**Tadaki and Inoue**

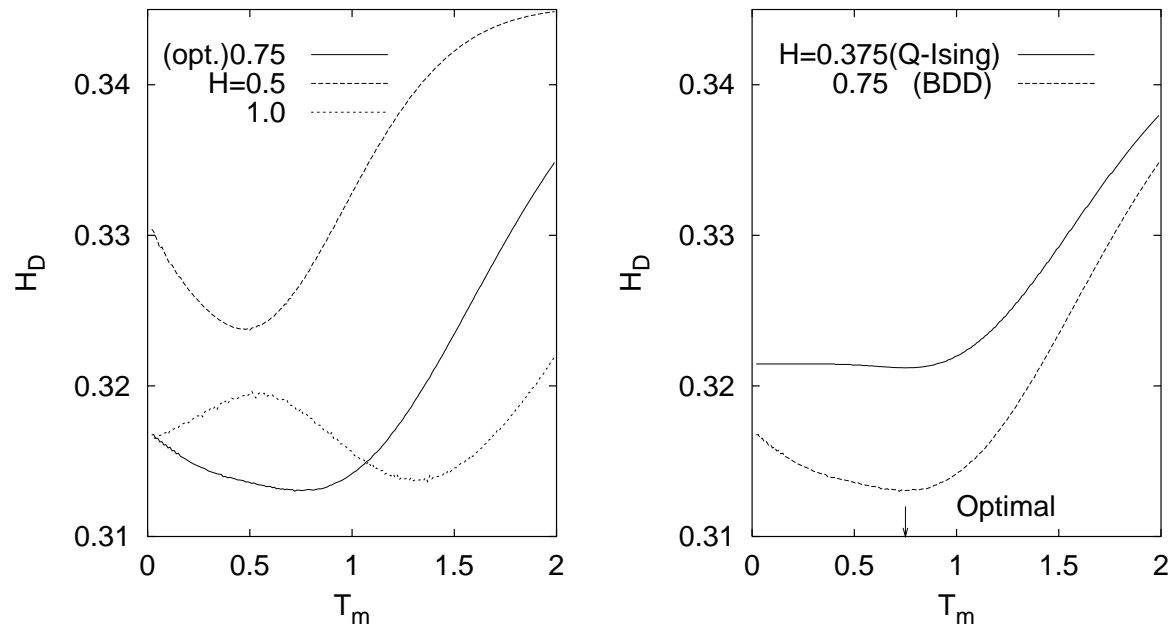
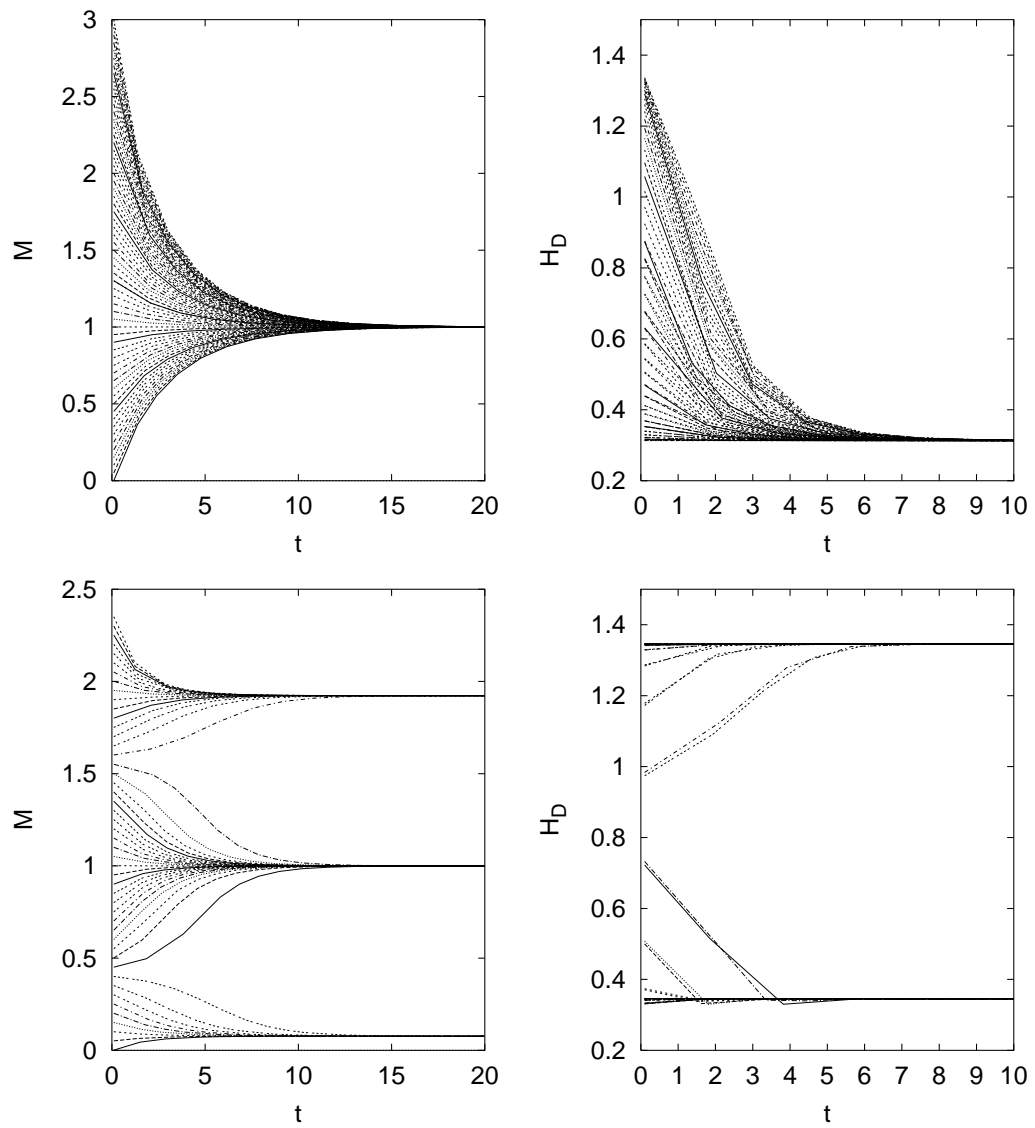


FIG. 6  
Tadaki and Inoue



**FIG. 7**  
**Tadaki and Inoue**

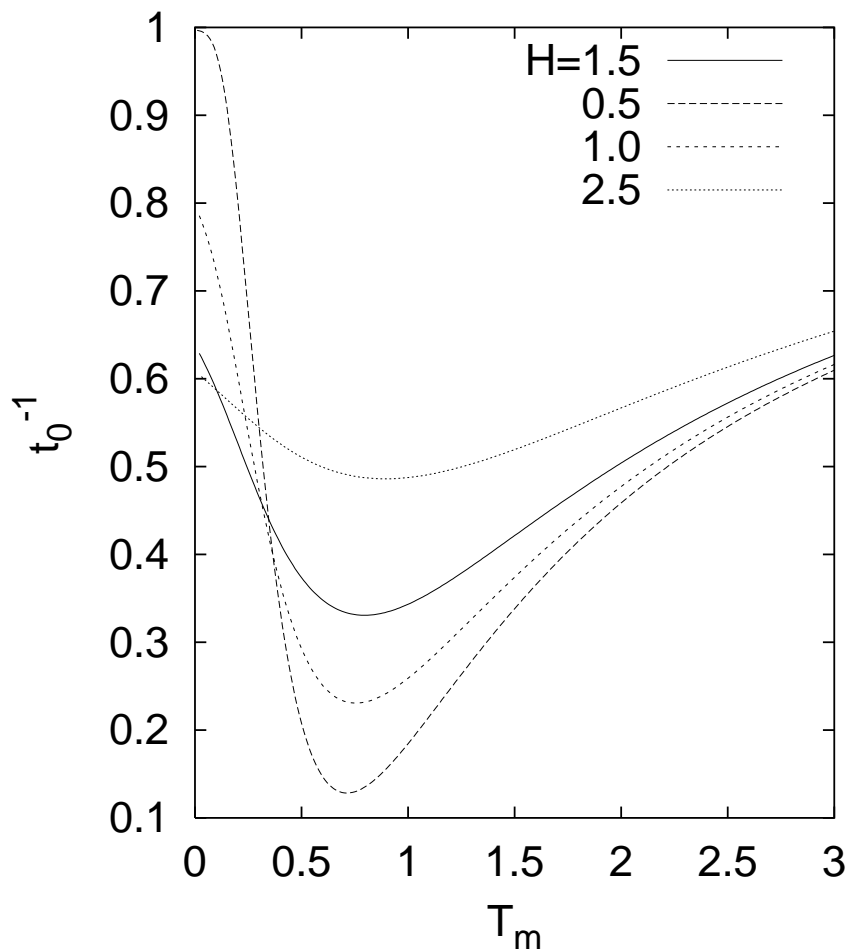


FIG. 8  
Tadaki and Inoue

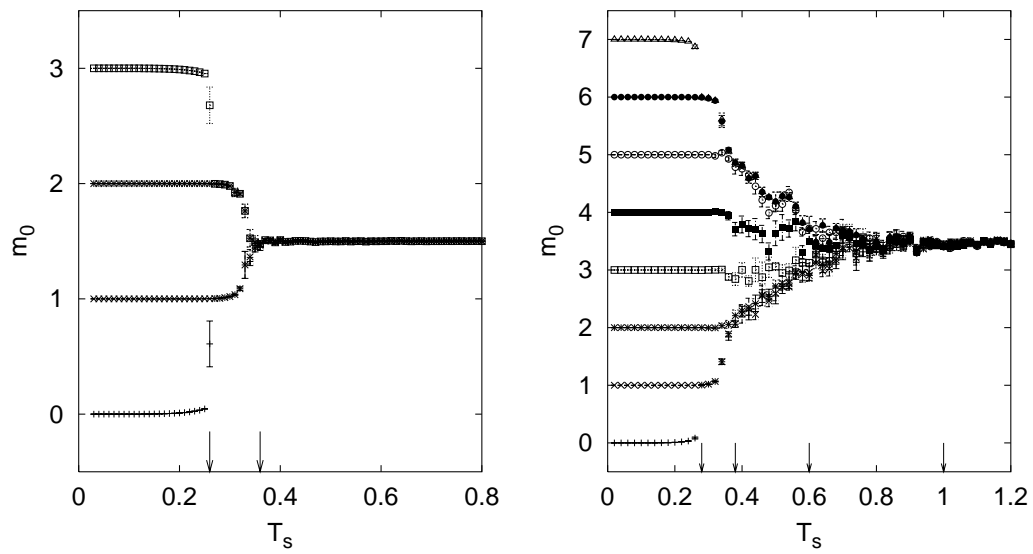


FIG. 9  
Tadaki and Inoue

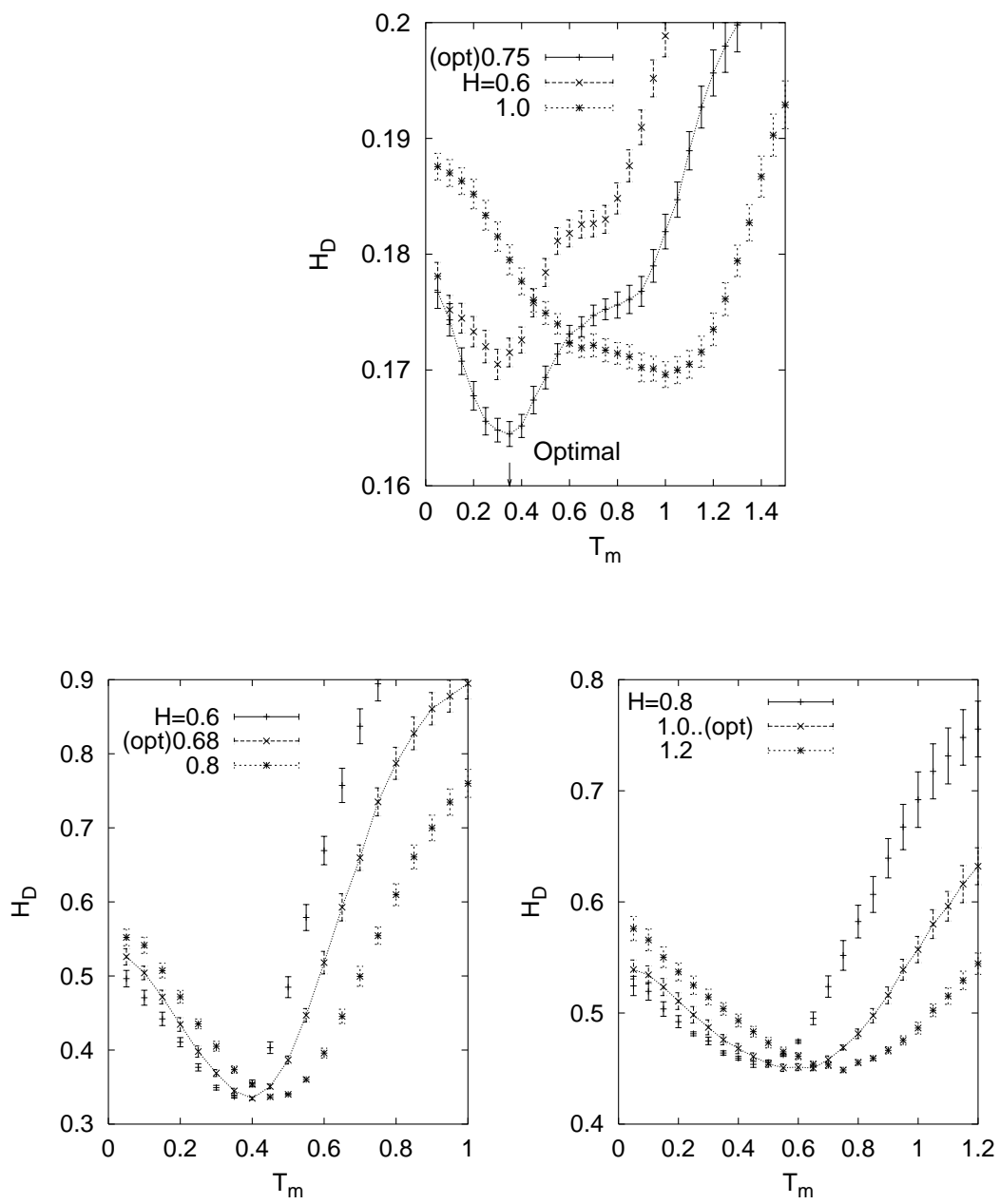
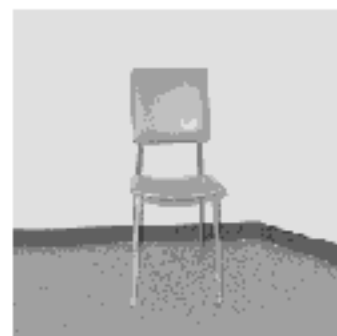


FIG. 10

Tadaki and Inoue



"chair"



"girl" (left) and "house" (right)



"lens" (left) and "mask" (right)

**FIG. 11**  
Tadaki and Inoue



Original image



Degraded images



Restored images

**FIG. 12**

Tadaki and Inoue



Original image



Degraded images



Restored images

FIG. 13

Tadaki and Inoue

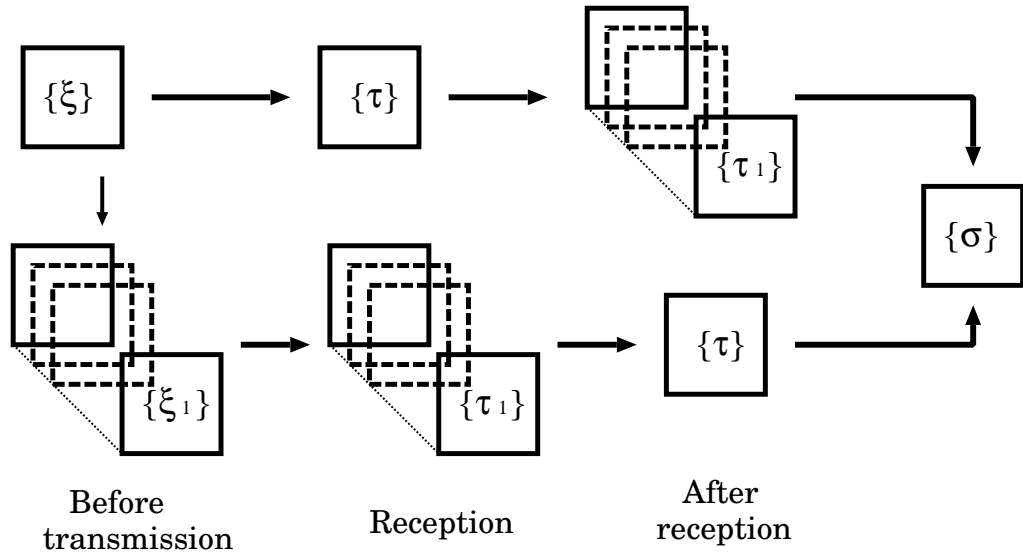


**FIG. 14**  
**Tadaki and Inoue**



**FIG. 15**  
**Tadaki and Inoue**